

Probabilistic Risk Assessment of Station Blackouts in Nuclear Power Plants

Hindolo George-Williams , Min Lee, and Edoardo Patelli 

Abstract—Adequate ac power is required for decay heat removal in nuclear power plants. Station blackout (SBO) accidents, therefore, are a very critical phenomenon to their safety. Though designed to cope with these incidents, nuclear power plants can only do so for a limited time, without risking core damage and possible catastrophe. Their impact on a plant's safety are determined by their frequency and duration, which quantities, currently, are computed via a static fault tree analysis that deteriorates in applicability with increasing system size and complexity. This paper proposes a novel alternative framework based on a hybrid of Monte Carlo methods, multistate modeling, and network theory. The intuitive framework, which is applicable to a variety of SBOs problems, can provide a complete insight into their risks. Most importantly, its underlying modeling principles are generic, and, therefore, applicable to non-nuclear system reliability problems, as well. When applied to the Maanshan nuclear power plant in Taiwan, the results validate the framework as a rational decision-support tool in the mitigation and prevention of SBOs.

Index Terms—Accident recovery, Monte Carlo simulation (MCS), nuclear power plant, risk assessment, station blackout (SBO).

NOTATIONS

$\min(\mathbf{B})$ Least element of set/vector \mathbf{B} .
 $\min\{\mathbf{B}, \mathbf{Q}\}$ Least element of $\mathbf{B} \cup \mathbf{Q}$.
 (\mathbf{B}, i) i th element of set/vector \mathbf{B} .

ABBREVIATIONS

AC Alternating Current.
 DC Direct Current.
 C Node capacity.
 CCF Common-cause failure.
 CCG Common-cause group.
 CS Cold standby state.
 F Failed state.
 LOOP Loss of offsite power.
 MCS Monte Carlo simulation.

Manuscript received October 6, 2017; revised December 7, 2017; accepted April 3, 2018. This work was supported by the EPSRC and ESRC Centre for Doctoral Training on Quantification and Management of Risk and Uncertainty in Complex Systems and Environments under Grant:EP/L015927/1. Associate Editor: W.-T. K. Chien. (Corresponding author: Edoardo Patelli.)

The authors are with the Institute for Risk and Uncertainty Engineering, University of Liverpool, Liverpool L69 3BX U.K., and also with the Institute of Nuclear Engineering and Science, National Tsing Hua University, Hsinchu City 300, Taiwan (e-mail: H.George-Williams@liverpool.ac.uk; mlee@ess.nthu.edu.tw; Edoardo.Patelli@liverpool.ac.uk).

Color versions of one or more of the figures in this paper are available online at <http://ieeexplore.ieee.org>.

Digital Object Identifier 10.1109/TR.2018.2824620

S	Shutdown state.	39
SBO	Station blackout.	40
SU	Start-up state.	41
TM	Test/preventive maintenance state.	42
W	Working state.	43
	NOMENCLATURE	44
A	System adjacency matrix.	45
C	Component capacity vector.	46
$c_x^{\{i\}}$	Capacity of component i in state x .	47
$\{c_x^{\{i\}}\}_{M \times 1}$	Set of current capacities of all components.	48
\mathbf{E}_i	Set of attributes of component i .	49
e	System edge matrix.	50
f_l	LOOP frequency.	51
f_s	SBO frequency.	52
$f_{xy}(t)$	Probability density function for transition from state x to y .	53
G	System graph object.	55
k	Number of edges/links in system graph.	56
lb	Set of minimum flow through edges/links.	57
M	Number of system nodes.	58
m	Number of safety buses/trains.	59
N	Number of Monte-Carlo samples.	60
n_1	Number of trains a generator can supply.	61
p_n	SBO probability given the $(n - 1)$ th SBO.	62
ub	Set of maximum flow through edges/links.	63
r	Number of components affected by a CCF.	64
$r_n(t)$	Non-recovery probability from the n th SBO.	65
S	Register indicating SBO occurrence.	66
s	Set of source nodes.	67
s_j	SBO indicator for the j th simulation sample.	68
T	Component transition matrix.	69
t	ID of virtual output node.	70
U_{tm}	Unavailability due to test or maintenance.	71
u	Proportion of train demand generator satisfies.	72
V	Set of nodes in the system graph.	73
x_0	Initial component state.	74
X_{ij}	Flow from node i to j .	75
X_{out}	Flow into the virtual output node.	76
Y	Set containing flows through all the nodes.	77
Θ	System inequality constraint matrix.	78
Γ	System incidence matrix.	79
Φ	System equality constraint matrix.	80
Ω_{ij}	Maximum flow from node i to j .	81
$\tilde{\delta}$	Number of intermediate nodes.	82
Ψ	System flow objective function.	83

84	ρ	Set of components making up CCG.
85	δ	Number of components in CCG.
86	θ	Set of CCF probabilities.
87	β_1	Common failure mode for CCG.
88	β_2	State rendering CCG vulnerable to CCF.
89	τ	Vector of next node transition times.
90	μ_{old}	Vector of node capacities at last system jump.

91 I. INTRODUCTION

92 **N**UCLEAR power is produced by harnessing the heat gen-
 93 erated from a fission reaction chain in a reactor vessel.
 94 The reactor vessel is placed in a concrete containment to shield
 95 the environment from the potential release of radioactive materi-
 96 als. Core damage ensues when the core temperature exceeds a
 97 certain threshold or the nuclear fuel elements in the vessel are
 98 uncovered. This event may trigger containment breach, inflict-
 99 ing huge environmental and economic catastrophe.

100 Severe accident mitigation is achieved in part by ensuring
 101 a reliable cooling water circulation in the reactor vessel. This
 102 objective, during normal plant operation, is achieved through
 103 heat exchange between the primary and secondary loops of the
 104 plant's main cooling system. The process, however, ceases on
 105 plant shut down and backup cooling systems are required to
 106 sustain decay heat removal. Like the main cooling system, the
 107 backup cooling systems rely on ac power provided by sources
 108 outside the plant (offsite power). When these sources fail (loss
 109 of offsite power—LOOP), emergency sources onsite are started,
 110 to drive the plant's safety systems. If the emergency sources are
 111 also unavailable or unable to function as required, the plant
 112 is said to be in a station blackout (SBO). The backup cool-
 113 ing systems, however, are equipped with alternative turbine or
 114 diesel-driven pumps to help the plant cope with this incident.
 115 These systems, on the downside, require for monitoring and
 116 control, dc power from dc power banks. Their sustainability,
 117 therefore, regardless of their inherent reliability, is limited by
 118 the dc battery depletion time. This time, and the boil-off rate
 119 of reactor coolant, define the maximum acceptable ac power
 120 recovery duration [1].

121 SBO accidents are the largest contributor to nuclear power
 122 plant risk, accounting for over 70% of the core damage fre-
 123 quency at some plants [1], [2]. LOOP events, which initiate
 124 these accidents, are classified on the basis of their origin. A grid-
 125 centred LOOP is due to the failure of the transmission network
 126 outside the plant, switchyard-centred LOOP arises from failures
 127 in the switchyard on the plant premises, plant-centered LOOP is
 128 triggered by the operational dynamics of the plant itself, while
 129 weather-related LOOP is attributed to failures induced by severe
 130 and extreme weather, excluding lightning [1], [2]. The effective
 131 SBO risk is the sum of the core damage frequencies induced by
 132 the various LOOP types.

133 A. Review of Existing Models

134 SBO risk quantification starts with a LOOP event tree analysis
 135 [3], where the emergency power system availability is checked
 136 in the first heading. This event failure, frequency of which de-
 137 fines the SBO frequency, transfers the analysis to the SBO event

tree [1]. In the latter, the successes of the various mitigating ac-
 138 tions, including offsite power and the recovery of the emergency
 139 diesel generators (EDGs) at specific times are also checked.
 140 These times, however, vary across plants and depend on the
 141 status of a plant's mitigating systems. At the Maanshan nuclear
 142 power plant, for instance, power recovery is checked at 1, 2,
 143 4, and 10 h into SBO. Each top event probability in the SBO
 144 event tree requires one or more static fault trees [4]–[6] for its
 145 quantification.
 146

Static fault tree analysis employs an analytical approach, as
 147 such, it carries the important advantage of being computationally
 148 efficient. For this reason, its sensitivity, importance, and un-
 149 certainty analysis capabilities are outstanding. These attributes
 150 explain its wide use for risk analysis in the nuclear, aviation [7],
 151 and chemical process industries [8]. Unfortunately, fault trees
 152 become intractable with large systems or moderate systems with
 153 complex interactions [8]. They often require a detailed knowl-
 154 edge of the system being modeled, making them both difficult
 155 to apply and error-prone. Their static nature also limits their
 156 applicability in many ways. For instance:

- 157 1) Implementing certain types of interdependencies is either
 158 tedious or completely impossible.
- 159 2) The analyst has to assume that SBO is coincident with
 160 LOOP and that all power recovery efforts start simultane-
 161 ously **after** SBO sets in. As a consequence:
 162 a) The SBO frequency and nonrecovery probability
 163 are overestimated in most cases, since the repair of
 164 a failed element is normally initiated immediately.
 165 b) For plants with multiple emergency power systems,
 166 it is impossible to determine which sequence of re-
 167 sponse minimizes the SBO frequency and maxi-
 168 mizes the recovery probability simultaneously.
 169 c) It is also difficult to investigate the effects of external
 170 factors like logistic problems, extreme environmen-
 171 tal events, and human resource constraints on the
 172 recovery process.
- 173 3) The analyst is forced to assume the nonoccurrence of
 174 a second SBO after power recovery. This assumption,
 175 however, loses its validity if the emergency sources are
 176 recovered first. In this case, a second failure could initiate
 177 another SBO sequence before offsite power recovery.
 178 4) Finally, there is the problem of inconvenience due to repet-
 179 itive modeling. Since the nonrecovery probability is nor-
 180 mally required for multiple instances, each would require
 181 a dedicated fault tree.
 182

183 There are numerous instances of remarkable attempts at ex-
 184 tending the applicability of fault trees to systems with interde-
 185 pendencies and various forms of dynamic interactions [6], [9].
 186 Kaiser *et al.* [10], for instance, introduced a state/event fault tree
 187 approach that translates fault-trees to deterministic and stochas-
 188 tic petri nets. Similarly, Zhou and Zhang [11], quite recently,
 189 proposed an approach that converts static fault trees to dynamic
 190 uncertain causality graphs in order to tackle the dynamic and un-
 191 certainty attributes of practical engineering systems. However,
 192 like Kaiser's approach [10], Zhou's [11] is restricted to binary-
 193 state components and systems. Even though the performance
 194 of most components could be partitioned into two levels, the

195 existence of multiple failure modes makes binary-state models
 196 inadequate. Also, from a modeling perspective, there are oc-
 197 casions when the analyst would need to model a binary-state
 198 element as a multistate one in order to fully define its behav-
 199 ior. Such flexibility requires a framework supporting multistate
 200 modeling. Bobbio *et al.*'s fault tree to Bayesian Network map-
 201 ping procedure [12] effectively solve this problem. However,
 202 like Kaiser's and Zhou's approaches, Bobbio's mapping pro-
 203 cedure is also susceptible to deficiencies (3) and (4) outlined
 204 above.

205 Dynamic fault trees [13]–[16] are perhaps the closest re-
 206 searchers have come to solving the limitations of static fault
 207 trees. Various approaches have been proposed for their solution
 208 but Markov analysis [14], [15], [17] remains the most popu-
 209 lar. Markov modeling, however, like static fault tree analysis,
 210 becomes intractable with large systems and is only applicable
 211 to exponentially distributed transitions. Nevertheless, state ex-
 212 plosion is no longer an issue, with the introduction of intuitive
 213 dynamic fault tree software [18], [19]. Even with these devel-
 214 opments, most of the dynamic fault tree solution approaches
 215 are susceptible to deficiencies (3) and (4) outlined above. These
 216 deficiencies can only be addressed by approaches offering the
 217 flexibility to replicate the exact behavior of the system. Such an
 218 approach, however, was put forward by Rao *et al.* [16], which
 219 they used to model the power supply system of a nuclear power
 220 plant. The approach simulates a system's dynamic fault tree and
 221 addresses most of the limitations of static fault trees. However,
 222 like the majority of system reliability models, Rao's work is
 223 only applicable to binary-state components. The development of
 224 a more universal simulation framework, therefore, is desirable.

225 B. Proposed Approach and Scope

226 As evidenced in Rao *et al.*'s [16], Rocha *et al.*'s [20], and Lei
 227 *et al.*'s [21] works, Monte Carlo simulation (MCS) is flexible
 228 enough to model any system attribute. Its problem, however, is
 229 that most of the existing MCS algorithms are system-specific
 230 and require either the structure function, cut sets, or path sets of
 231 the system. An intuitive event-driven MCS procedure, offering
 232 multistate component modeling opportunities has recently been
 233 proposed [22]. This procedure is general and does not require the
 234 definition of the system's path and cut sets or structure function,
 235 thanks to its embedded graph model.

236 In this work, the graph and multistate models proposed in
 237 [22] are adopted. The graph model is used to model the topol-
 238 ogy of the system and allow the performance of the system to
 239 be directly computed from the performance of the components.
 240 This attribute eliminates the need for an explicit association of
 241 component failure combinations to the state of the system. The
 242 multistate model, on the other hand, is used to model the behav-
 243 ior of the components, overcoming the assumption of a perfectly
 244 binary behavior of components. It is particularly useful to the
 245 multiple failure mode and dynamic attribute representation of
 246 the emergency power systems. This model, for instance, could
 247 be exploited to investigate the effects of limited maintenance
 248 teams or the unavailability of spares on the emergency power
 249 systems recovery [23]. We extend the original model to incorpo-
 250 rate interdependencies by means of a dependency matrix and an

efficient recursive algorithm to propagate the effects of failures
 across the system. Completing the framework, we propose a
 simple MCS algorithm that induces LOOP in the system, repli-
 cate the ensuing sequence of events, and monitor the availability
 of power at the various safety buses. The number of available
 safety buses, as a function of time, is computed after each sys-
 tem event. From the simulation history, any SBO index can be
 computed, thereby providing an opportunity for more insights
 into SBO risks. The multistate component model, together with
 the dependency matrix, adequately captures and represents the
 redundancies in the emergency power system of the plant. Con-
 sequently, the explicit modeling of these redundancies, which
 poses a significant challenge, is eliminated.

1) *Merits and Novelty of the Proposed Approach:* The
 framework, for now, is limited to grid and switchyard induced
 LOOP, given their dominance [2]. Its preliminary results were
 first presented at the 13th Probabilistic Safety Assessment and
 Management conference [24]. However, this paper proposes
 several improvements. First, an extensive review of the suitabil-
 ity of fault trees and their derivatives, to SBO analysis has been
 included. We have also considered the effects of common-cause
 failures (CCF), unavailability due to test or maintenance, and
 human error on the SBO frequency and recovery probability. We
 also show how the results obtained from the framework can be
 absorbed in the existing model. Finally, we extend the number
 of computable SBO indices and consider the effects of system
 configuration and the sequence of operator response on system
 recovery.

This paper is the first documented application of load-flow
 simulation to a complete SBO risk assessment. With respect
 to the existing models discussed in Section I-A, the proposed
 framework exhibits the following advantages:

- *Adequacy and Flexibility:* It models realistic attributes of
 the plant's power recovery and provides more insights into
 SBO risks. For instance, it enhances the investigation of
 the possibility of a second SBO after the first.
 - *Convenience and Generality:* It is convenient in the sense
 that the modeler does not need to deduce the combination
 of component failure leading to system failure. They also
 do not need to explicitly model component redundancies,
 as these are implicitly captured by the modeling frame-
 work. The modeling framework, in addition, is applicable
 to many system reliability problems.
- 2) *Solution Sequence:* The proposed approach is applied as
 summarized by the following chronological steps:
- Identify the key elements of the system, define its topology,
 and derive its flow equation parameters.
 - Develop the multistate model for each system element.
 - Model the interdependencies between the elements.
 - Force a LOOP event and simulate the behavior of the
 standby power systems.
 - Compute the SBO indices from the simulation history.

II. SBO MODELING

A nuclear power plant's power system consists of the grid,
 the switchyard, the emergency power systems, alternative emer-
 gency power system, and the safety buses. The alternative

307 emergency power systems are additional emergency sources
 308 [such as gas turbine generators (GTGs)] available at some plants
 309 to boost their LOOP/SBO recovery capability. In this section,
 310 we show how the plant's power system is accurately modeled
 311 and analyzed, in line with the solution sequence outlined in
 312 Section I-B2.

313 A. System Topology

314 We represent the topology of the plant's power system by
 315 a graph nodes of which depict the components of the system.
 316 Connecting the nodes are perfectly reliable links portraying
 317 the direction of power flow. Flows from all the safety buses
 318 are terminated on a virtual node, introduced to represent the
 319 total available power. This virtual node would later be used to
 320 compute the nonrecovery probability of ac power.

321 Let the nodes of the system be numbered from 1 to M and
 322 represented by the set $\mathbf{V} = \{1, 2, \dots, M\}$. Since the links are
 323 perfectly reliable, the adjacency matrix, \mathbf{A} , of the system is
 324 defined as

$$\mathbf{A} = \{a_{ij}\}_{M \times M} \mid a_{ij} = \begin{cases} 1 & \text{If flow is } i \rightarrow j \\ 0 & \text{Otherwise.} \end{cases} \quad (1)$$

325 The topology of the system, therefore, can be defined by $G \mid$
 326 $G = (\mathbf{V}, \mathbf{A})$. Using the parameters of G only, the flow equations
 327 of the system can be derived [22]. These equations can then be
 328 used in synergy with the current state properties of the system
 329 nodes to deduce the performance of the system. For this, a linear
 330 programming algorithm is employed, given the possibility of flow
 331 redirection and the need to satisfy the capacity constraints of
 332 the nodes and their links. The objective is to find the flow across
 333 each link of the system that maximizes the flow into the virtual
 334 node. If X_{ij} is the flow across the link between nodes i and
 335 j and given there are k such links for all $(i, j) \in \mathbf{e}$, where \mathbf{e}
 336 is the edge matrix of the system as defined in [22], the linear
 337 programming problem is formulated by (2), (5), (7), and (8)

$$\Theta \{X_{ij}\}_{k \times 1} \leq \{c_x^{(i)}\}_{M \times 1} \mid (i, j) \in \mathbf{e} \quad \forall i \in \mathbf{V}. \quad (2)$$

338 Equation (2) expresses the inequality constraints to be satisfied,
 339 where $c_x^{(i)}$ denotes the capacity of node i when residing in state
 340 x . $\{c_x^{(i)}\}_{M \times 1}$, therefore, is the vector of current capacities of all
 341 the nodes of the system. The inequality matrix, Θ , is related to
 342 the incidence matrix, Γ , as follows:

$$\Theta = \{\theta_{iq}\}_{M \times k} \mid \theta_{iq} = \begin{cases} 1, & \gamma_{iq} \neq 0 \\ 0, & \text{otherwise} \end{cases} \quad (3)$$

$$\Gamma = \{\gamma_{pq}\}_{M \times k} \mid \gamma_{pq} = \begin{cases} 1, & p = i \\ -1, & p = j \\ 0, & \text{otherwise.} \end{cases} \quad (4)$$

343 Γ is related to \mathbf{A} by (4), where $q = 1, 2, \dots, k$ (the edge number)
 344 is the index of the edge between nodes i and j in \mathbf{e} and $p =$
 345 $1, 2, \dots, M$

$$\Phi \{X_{ij}\}_{k \times 1} = \{0\}_{\bar{\delta} \times 1} \quad \forall (i, j) \in \mathbf{e}. \quad (5)$$

Equation (5) expresses the equality constraint to be satisfied, 346
 where Φ and Γ are related, thus 347

$$\Phi = \{\phi_{\lambda q}\}_{\bar{\delta} \times k} \mid \phi_{\lambda q} = \gamma_{pq} \\ \lambda = 1, 2, \dots, \bar{\delta} \mid \bar{\delta} < M \quad f : \lambda \rightarrow p \quad \forall p \in (\mathbf{s} \cup \mathbf{t})'. \quad (6)$$

$\bar{\delta}$ is the number of intermediate nodes, \mathbf{s} is the set of source 348
 nodes, which comprises the grid and standby power systems, 349
 while \mathbf{t} is the virtual node representing the total output of the 350
 system. If the intermediate nodes of the system (i.e., nodes not in 351
 \mathbf{s} and \mathbf{t}) are arranged in ascending order of their ID, (6) suggests 352
 the λ th row of Φ is identical to the p th row of Γ , where p is the 353
 λ th element of the ordered set of intermediate nodes. In other 354
 words, Φ is a submatrix of Γ , containing all the rows of the 355
 latter corresponding to intermediate nodes 356

$$\mathbf{lb} = \{0\}_{k \times 1}, \quad \mathbf{ub} = \{\Omega_{ij}\}_{k \times 1} \\ \Omega_{ij} = \min\{c_{\max}^{(i)}, c_{\max}^{(j)}\} \quad \forall (i, j) \in \mathbf{e}. \quad (7)$$

Equation (7) defines the lower and upper bound vectors, \mathbf{lb} and 357
 \mathbf{ub} , of the flow through the links, where $c_{\max}^{(i)}$ is the maximum 358
 capacity of node i . Finally, the objective function of the linear 359
 programming problem is expressed as 360

$$\Psi = -\{\psi_q\}_{1 \times k} \{X_{ij}\}_{k \times 1} \mid \psi_q = \sum_{i \in \mathbf{s}} \gamma_{iq}. \quad (8)$$

Following the termination of the linear programming algorithm, 361
 the vector of flow, \mathbf{Y} , through the nodes of the system is given 362
 by $\Theta_{M \times k} \{X_{ij}\}_{k \times 1}$. The total output, therefore, is given by the 363
 t th element, (\mathbf{Y}, \mathbf{t}) , of \mathbf{Y} . Interestingly, all the parameters, but 364
 $\{c_x^{(i)}\}_{M \times 1}$, required to compute \mathbf{Y} remain static during system 365
 simulation. The main task, therefore, is to update $\{c_x^{(i)}\}_{M \times 1}$ after 366
 each system event. The derivation of (2) to (8) is outside the 367
 scope of this paper, interested readers are referred to [22]. How- 368
 ever, an illustrative example of the linear programming problem 369
 formulation is provided in the Appendix of this paper. 370

371 B. System Components

Each component is defined by a multistate model that takes 372
 into account the various parameters that characterize its opera- 373
 tion. Let E_i denote component i , then 374

$$E_i = (\mathbf{T}, \mathbf{C}, x_0) \quad (9)$$

$$\mathbf{T} = \{T_{xy}\}_{n \times n} \mid x \neq y \quad (x, y) \in \{1, 2, \dots, n\},$$

$$T_{xy} = \begin{cases} \infty, & \text{If } x \rightarrow y \text{ is a forced transition} \\ 0, & \text{If no transition between states } x \text{ and } y \\ f_{xy}(t), & \text{Otherwise} \end{cases} \quad (10)$$

where \mathbf{T} is the transition matrix of the component; $\mathbf{C} \mid \mathbf{C} =$ 375
 $\{c_x\}_{1 \times n}$ is the capacity vector; x_0 is the initial state; c_x is the 376
 capacity in state x ; n is the number of states; and $f_{xy}(t)$ is the 377
 probability density function characterizing the transition from 378
 state x to y . \mathbf{T} contains the density function objects for all the 379
 transitions depicted in the multistate model of the component 380
 and \mathbf{C} defines the capacity of the component in each state. 381

382 Each state capacity is expressed as a nondimensional number
 383 defining the proportion of total system output the node can
 384 supply or transmit while residing in that state. If m is the total
 385 number of power trains at the plant, n_1 , the number of power
 386 trains the node simultaneously supplies, u , the proportion of
 387 power train demand it can satisfy, then, its capacity when work-
 388 ing perfectly is, $n_1 u m^{-1}$. It expresses the total system output as
 389 a fraction of the number of power trains/safety buses present at
 390 the plant. On this note, the grid and switchyard nodes are each
 391 assigned unity capacity when available and 0, otherwise. The
 392 virtual output node has a fixed capacity of 1 and each safety bus,
 393 a fixed capacity of m^{-1} .

394 1) *Modeling the Grid and Switchyard:* The grid is modeled
 395 as a two-state node: “Working,” when available and “Failed,”
 396 otherwise. Though grid failures are mostly random, we model
 397 them as forced transitions [23], since they already are incorpo-
 398 rated in the LOOP frequency. Most often, plants tap their ac
 399 power from multiple offsite sources, and grid failure is defined
 400 as the failure of all of these sources. The repair of at least one of
 401 the failed sources, however, is sufficient to achieve grid recov-
 402 ery. For this reason, the transition from “Failed” to “Working”
 403 is defined by the upper bound of the envelope around the cumu-
 404 lative density functions (cdf) of the individual source repair
 405 distributions. Given this, sampling the grid recovery time entails
 406 generating a uniform random number and reading off its corre-
 407 sponding time from the envelope cdf, interpolating where neces-
 408 sary. An important point to note is that this approach slightly
 409 underestimates the grid recovery probability, as it assumes the
 410 individual source repair actions are initiated concurrently. In
 411 practice, the sources do not necessarily fail simultaneously and
 412 their recovery actions may commence at different times. This
 413 implies, by the time the last source fails, the restoration of
 414 already failed sources would have begun. The actual grid recov-
 415 ery time, therefore, is less than that given by the envelope
 416 cdf. This, however, is acceptable, as the goal in risk manage-
 417 ment is to ensure risk levels are acceptable, even in worst case
 418 scenarios.

419 Similarly, normal switchyard operation is defined by a two-
 420 state node. In cases where the plant is enhanced with multiple
 421 switchyards, switchyard recovery is treated as in the case of
 422 multiple grid sources. Fig. 1 shows the multistate model for the
 423 grid and switchyard.

424 2) *Modeling the Standby Power Systems:* The emergency
 425 power system is constituted by the EDGs, and in this work,
 426 GTGs constitute the alternative emergency power system. In this
 427 section, we model only the multistate behavior of the standby
 428 power systems, and the effects of redundancies on their opera-
 429 tion is considered in a latter section. We make the following
 430 assumptions in developing these models.

- 431 1) The initiation of test/maintenance is coincident with
 432 LOOP, and at any instance, there is not more than one
 433 source in test or maintenance.
- 434 2) Sources in test or maintenance remain unavailable through-
 435 out the sequence.
- 436 3) Repairs are commenced immediately.
- 437 4) A generator just from maintenance cannot fail to start.
 438 This implies a perfect maintenance scenario.

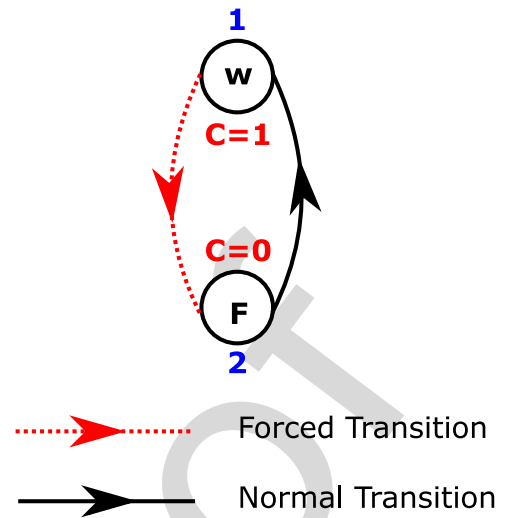


Fig. 1. Multistate model for grid and switchyard nodes.

439 The alternative emergency power system recovery is assumed
 440 offsite power recovery in [24]. This assumption is on the premise
 441 that their failure is included in the LOOP frequency. However,
 442 the assumption is impractical, given they are mostly a standby
 443 source. We, therefore, modify their multistate model to include
 444 running failures, rendering them an onsite source.

445 We consider failure-to-start and failure-to-run as the only fail-
 446 ure modes an EDG is susceptible to. Failure-to-start refers to
 447 the EDG failure to start from cold-standby and failure-to-run
 448 denotes its failure to function for the duration of the LOOP.
 449 While the former is defined by a crisp probability, the latter is
 450 characterized by a time-to-failure probability density function.
 451 However, the standardized plant analysis risk model [1] consid-
 452 ers a third EDG failure mode, failure-to-load, defining the case
 453 when the EDG starts but cannot power the load. This failure
 454 mode is considered failure-to-start, in the proposed framework.
 455 We introduce two additional states, “Working” and “TM,” as
 456 shown in Fig. 2, to account for the perfect operation of the EDG
 457 and its unavailability due to test or maintenance, respectively.
 458 Except otherwise, the transition from cold standby to working is
 459 instantaneous, while the transition from cold standby to failure
 460 or TM is also instantaneous but conditional. Conditional transi-
 461 tions are a special type of forced transition depending on a
 462 probabilistic event that is external to the component and with a
 463 known likelihood [23]. Conditional and forced transitions have
 464 the same representation in the transition matrix of the compo-
 465 nent [see (10)].

466 The GTGs behave in almost the same way as the EDGs, save
 467 for the difference in their start-up and manual alignment times.
 468 For this, a start-up state is inserted between their cold-standby
 469 and working states, as shown in Fig. 2. While in start-up, they
 470 could fail, explaining the transition from start-up to failure.

471 3) *Accounting for Human Error:* Human error is very im-
 472 portant in the risk assessment of engineering systems. In SBO
 473 recovery, human errors mostly manifest themselves as delayed
 474 response to certain SBO mitigation action. For instance, the
 475 switchyard is forced into a temporary shutdown state during grid

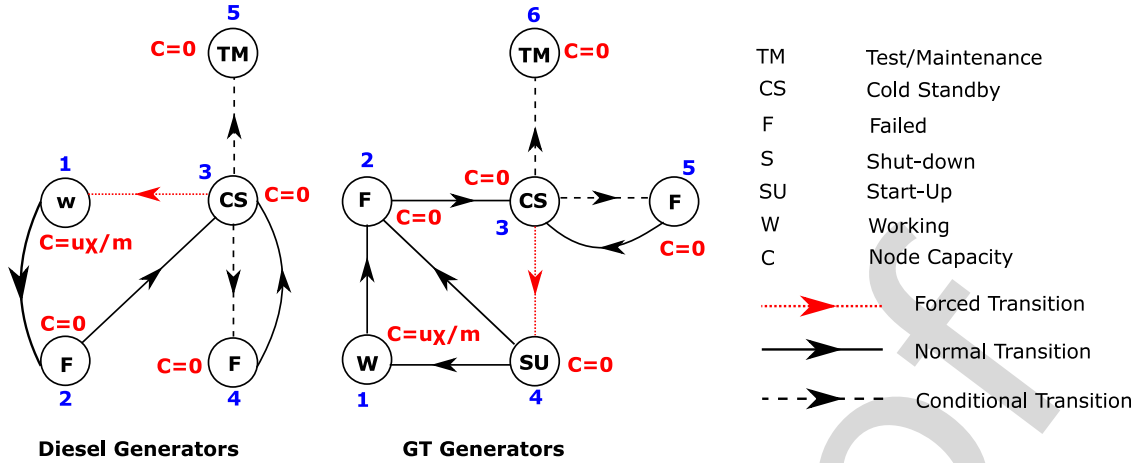


Fig. 2. Multistate models for emergency diesel and GTGs without human error consideration.

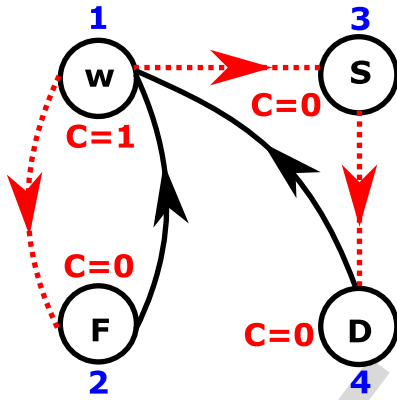


Fig. 3. Multistate model for switchyard with human error consideration.

476 failures. On grid recovery, the plant personnel manually initiate
 477 its restoration, which process is susceptible to human-induced
 478 delays. Accounting for these delays, two additional states are
 479 introduced in the two-state model discussed in Section II-B1,
 480 as shown in Fig. 3. The transitions from “Working” to “Shut-
 481 down” and from “Shutdown” to “Delay” (D), are influenced
 482 by grid failure and recovery respectively. “Shutdown” denotes
 483 grid recovery-in-progress, while “Delay” represents switching-
 484 in-progress. The latter determines the difference between the
 485 potential and actual bus recovery times. If this difference is neg-
 486 ligible or the potential, instead of the actual bus recovery time
 487 is required, the model in Fig. 1 is retained.

488 Similarly, the GTG and some EDGs require manual start-up
 489 and alignment, this is the case for shared diesel generators. A
 490 generator is said to be shared if it can substitute several units but,
 491 however, can only replace one unit at a given instance. There-
 492 fore, in the case of sequential multiple unit failures, only the
 493 first unit is replaced. For simultaneous failures, any of the units
 494 can be replaced, since they normally are identical. Since these
 495 replacements are manually executed, they are susceptible to del-
 496 lays, contrary to what most models suggest. Fig. 2, for instance,
 497 assumes the transition from cold standby to the fully functional
 498 or failure state to be instantaneous. This, by extension, implies,

any maintenance action (if the generator fails to start) is initiated
 499 at once. However, with human error, the start-up procedure
 500 may be initiated later than scheduled. We, therefore, introduce
 501 two states, one each, between cold standby and working and
 502 failure and cold standby, as shown in Fig. 4, to account for these
 503 delays. We have assumed the plant personnel to be well trained,
 504 experienced, and fit to perform their assigned tasks as expected.
 505 Consequently, the possibility of inappropriately executed ac-
 506 tions is ignored.
 507

Transitions $6 \rightarrow 1$ with $4 \rightarrow 7$ and transition $7 \rightarrow 4$ with $5 \rightarrow$
 508 8, of Fig. 4, account for human error in the recovery of manually
 509 operated emergency diesel and GTGs, respectively. In practical
 510 applications, human error is expressed in terms of the probability
 511 of not completing a given action within a specified time. If
 512 this probability is known for multiple times, a cdf could be
 513 fitted through the points. For this, we recommend the Weibull
 514 distribution, since it can yield a wide range of distributions.
 515 Recall the cdf of a Weibull distribution is $1 - e^{-(t/a)^b}$, where
 516 a and b are its scale and shape parameters, respectively. Given
 517 the human error probabilities are the likelihoods of inaction,
 518 they define the complement of the human reaction time cdf.
 519 Therefore, the Weibull parameters, a and b , are obtained by
 520 fitting the set of probability values to the function $e^{-(t/a)^b}$.
 521

C. Modeling Component Interdependencies

To ensure resilience, system designers often employ multi-
 523 ple layers of defense, either in the form of redundancies or
 524 shared components. This proactive strategy inadvertently intro-
 525 duces interdependencies in the system, resulting in modeling
 526 accuracy issues. We define interdependency in a more gener-
 527 al sense as the potential for a state change in one element
 528 to trigger a state change in another. We propose two models,
 529 the CCF and the cascading failure models, to implement these
 530 interdependencies.
 531

1) *CCF Model*: This model is used when the random failure
 532 of any member of a group of similar components, performing
 533 the same task could cause the failure of one or more of the
 534 remaining components [25]. Such a group of components is
 535

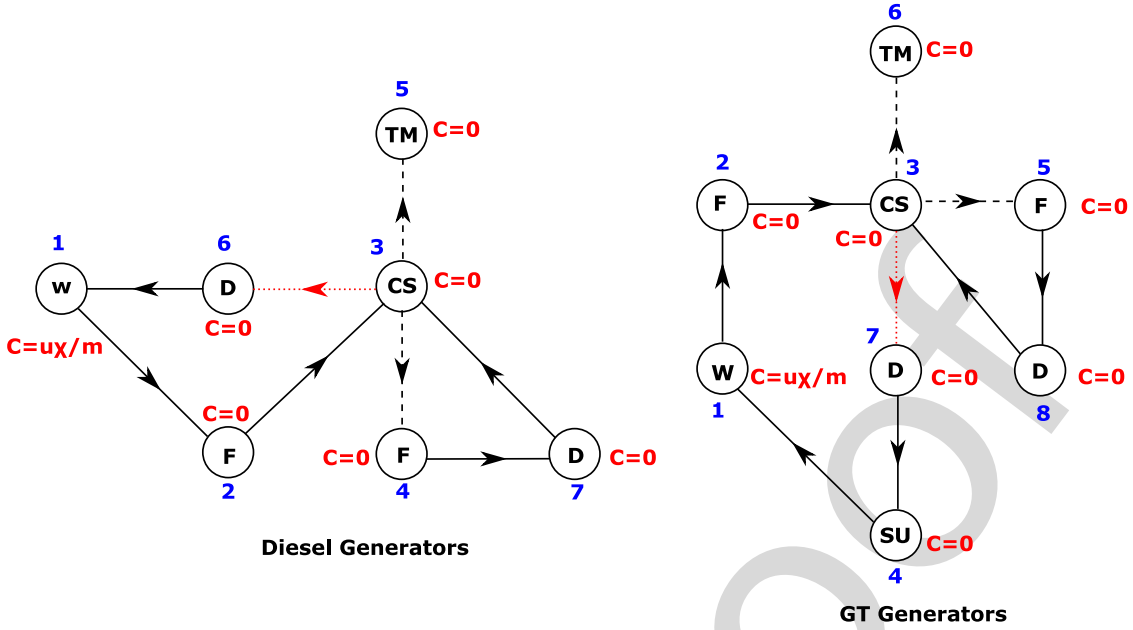


Fig. 4. Multistate models for emergency diesel and GTGs with human error consideration.

536 called a common-cause group (CCG), and its key attributes are
537 as follows:

538 1) There is a set of probabilities associated with the number
539 of components involved in any random failure event.
540 Let this set of probabilities be defined by $\theta \mid \theta = \{\theta_r\}^\delta$,
541 where r is the number of components affected by the failure
542 event, δ , the total number of components in the group,
543 and $\sum_{r=1}^{\delta} \theta_r = 1$.

544 2) All the components in the CCG fail in the same mode.
545 Implying, the CCG for start-up failures cannot influence
546 the CCG for running failures, for instance.

547 Each CCG, therefore, is defined by the quadruple,
548 $(\rho, \beta_1, \beta_2, \theta)$, where ρ is the set of components in the CCG,
549 β_1 , the common failure mode, and β_2 , the state the components
550 have to be in to be susceptible to this failure mode. The algorithm
551 for propagating CCF is summarized thus.

- 552 1) When a component fails, check if its new state matches
553 β_1 for its CCG.
- 554 2) Go to step (v) if there is no match. Else, determine the
555 number of components, r , that will fail.
- 556 3) Go to step (v) if $r = 1$. Else, remove from ρ , the component
557 initiating the failure event. From the remainder,
558 randomly select $r - 1$ components.
- 559 4) For each component selected in step (iii), check if its
560 current state matches β_2 and set this to β_1 .
- 561 5) End procedure.

562 The procedure above requires θ to be in conformity with
563 the α -Factor model [25]. CCF probabilities expressed in the
564 multiple Greek letter model would need to be converted as
565 in [25].

566 2) *Cascading Failure Model*: This model is used for inter-
567 dependencies not satisfying the CCF criteria. For instance, the
568 redundancies among the standby power systems and the de-
569 pendence of the latter on the grid and switchyard. An important

570 assumption invoked in this model, however, is that on occurrence
571 of the trigger event, the dependent event occurs immediately.

572 Initially proposed in [26], the model defines interdependen-
573 cies by a dependency matrix. The dependency matrix, \mathbf{D}_i , for
574 node i , defines the effects of the node's state transition on
575 other nodes. It takes the form, $\mathbf{D}_i = \{d_{j1}, d_{j2}, d_{j3}, d_{j4}\}_{v \times 4} \mid$
576 $j = 1, 2, \dots, v - 1, v$, where d_{j1} is the state of i triggering the
577 event, d_{j2} , the affected node, d_{j3} , the state the node has to be in
578 to be vulnerable, and d_{j4} , its target state after the event. Each row
579 of \mathbf{D}_i defines the behavior of an affected node, and v , the number
580 of relationships. For example, consider a two-component
581 system, with each component existing in three possible distinct
582 states. When component 1 makes a transition to state 3, component
583 2 is forced to make a transition to state 2 as well, if and only
584 if the latter is currently residing in state 1. Since component 1
585 is the trigger component in this case, the interdependency is
586 defined by \mathbf{D}_1 as

$$\mathbf{D}_1 = \begin{pmatrix} 3 & 2 & 1 & 2 \end{pmatrix}. \quad (11)$$

587 Let a third three-state component be added to the system. In
588 addition to its effect on component 2, let the transition of
589 component 1 also affect component 3, such that the latter is
590 forced to state 1 if it is in state 3 at the time of the trigger event.
591 To represent the overall behavior of component 1, \mathbf{D}_1 is updated
592 as shown in (12), to reflect the new information:

$$\mathbf{D}_1 = \begin{pmatrix} 3 & 2 & 1 & 2 \\ 3 & 3 & 3 & 1 \end{pmatrix}. \quad (12)$$

593 (12) shows that each row of the dependency matrix represents a
594 possible outcome.

595 Occasionally, a state change in a node can only affect another
596 node if a third node is in a certain state. This type of dependency
597 is known as a joint dependency, and it is outside the scope of the
598 initial model in [26]. We introduce the joint dependency matrix,

599 $\mathbf{D}' = \{d'_{j1}, d'_{j2}, d'_{j3}, d'_{j4}\}_{v \times 4}$, to resolve this problem. Element
 600 d'_{j1} defines the state the third node must be in to satisfy the joint
 601 dependency, while d'_{j2}, d'_{j3} , and d'_{j4} have the same meaning as
 602 d_{j2}, d_{j3} , and d_{j4} , respectively. Assuming a certain state change
 603 in node i only affects, say node x , if node ω is in state σ ,
 604 \mathbf{D}_i defines the relationship between nodes i and ω , while \mathbf{D}'_ω
 605 defines the relationship between ω and x . Nodes i, ω , and x are
 606 the trigger, intermediate, and target nodes, respectively. The
 607 intermediate node does not undergo a state change, meaning
 608 its target state is the same as its vulnerable state. Therefore, in
 609 \mathbf{D}_i , the third and fourth elements of the row corresponding to
 610 the intermediate node are equal. Given $j = 1$, for \mathbf{D}_i , $d_{12} = \omega$,
 611 $d_{13} = d_{14} = \sigma$ and for \mathbf{D}'_ω , $d'_{11} = \sigma$, $d'_{12} = x$. The remaining
 612 elements retain their meaning, as defined earlier. Let, for illus-
 613 trative purposes, the dependency between components 1 and 3
 614 (second row of \mathbf{D}_1 in (12)) only hold if component 2 is in state 2:

$$\mathbf{D}_1 = \begin{pmatrix} 3 & 2 & 1 & 2 \\ 3 & 2 & 2 & 2 \end{pmatrix} \quad \mathbf{D}'_2 = (2 \ 3 \ 3 \ 1). \quad (13)$$

615 To represent this attribute, the second row of \mathbf{D}_1 is modified
 616 to reflect the relationship between components 1 and 2, and the
 617 relationship between components 2 and 3, defined by \mathbf{D}'_2 as
 618 shown in (13). Notice \mathbf{D}'_2 , instead of \mathbf{D}_2 , has been used, since
 619 the relationship between components 2 and 3 is due to a joint
 620 dependency with another component.

621 The dependency and joint dependency matrices, indeed, can
 622 be used to represent a wide range of dependencies. However,
 623 there are a few instances that may result in large matrices. Such
 624 cases require an intuitive manipulation, to keep the matrix size
 625 moderate and prevent modeling error. We introduce a negative
 626 sign in front of the trigger or vulnerable state to signify that
 627 the dependency is satisfied only if the component is **not** in that
 628 state. This notation is analogous to the **NOT-gate** in fault trees.
 629 For instance, if component 1, in the scenario above, can affect
 630 component 3 only if component 2 is in states 2 or 1, it is efficient
 631 to exploit the **NOT** notation, instead of inserting an additional
 632 row in each of \mathbf{D}_1 and \mathbf{D}'_2 . Recalling that component 2 has 3
 633 states, state 2 **OR** state 1 is logically equivalent to **NOT** state 3.
 634 Hence, the dependency matrices, \mathbf{D}_1 and \mathbf{D}'_2 , become

$$\mathbf{D}_1 = \begin{pmatrix} 3 & 2 & 1 & 2 \\ 3 & 2 & -3 & -3 \end{pmatrix} \quad \mathbf{D}'_2 = (-3 \ 3 \ 3 \ 1).$$

635 We propose a recursive algorithm to implement the depen-
 636 dency matrices. If x_i denotes the new/current state of node i ,
 637 the algorithm is summarized thus.

- 638 i) Define a register, \mathbf{R} , to hold the affected components,
 639 their vulnerable, and target states.
- 640 ii) Using \mathbf{D}_i and x_i , find all components affected by the
 641 state change and update \mathbf{R} with elements 2 to 4 of the
 642 rows representing the components.
- 643 iii) Select the last row of \mathbf{R} and check if its last two elements
 644 are equal. This row defines the dependency induced in
 645 component ω by component i .
- 646 iv) If the response to the query in step (iii) is in the affirma-
 647 tive, designate the equal elements, ϵ , delete the last row
 648 of \mathbf{R} , and

- a) Using ω , \mathbf{D}'_ω , and x_ω as inputs, call steps (i) to
 649 (vii), noting that a row in \mathbf{D}'_ω is affected by the
 650 state change only if its first element is ϵ . 651
 - b) Continue from step (iii). 652
- Else, proceed to step (v). 653
- v) Force the designated transition as determined in step (iii)
 654 and delete the last row of \mathbf{R} . If the affected node is in
 655 standby, and its target state, working, delay, or start-up,
 656 initiate its start-up procedure. 657
 - vi) If \mathbf{D}_ω exists, repeat steps (ii) to (vi), replacing \mathbf{D}_i and
 658 x_i with \mathbf{D}_ω and x_ω , respectively. 659
 - vii) Repeat steps (iii) to (vi) until \mathbf{R} is empty, and terminate
 660 the procedure. 661

III. SYSTEM SIMULATION AND ANALYSIS 662

663 The system's operation is imitated by generating random fail-
 664 ure events of components and their corresponding repairs. For
 665 every component transition, the capacity vector, $\{c_x^{\{i\}}\}_{M \times 1}$, of
 666 the system is updated and used to deduce the flow, (\mathbf{Y}, \mathbf{t}) ,
 667 through the output node. At time $t = 0$, the grid and switch-
 668 yard nodes are in operation, while the emergency power systems
 669 and alternative emergency power systems are in cold standby.
 LOOP is initiated by setting the grid (for grid centred LOOP)
 670 or the switchyard (for switchyard centred LOOP) to its failure
 671 state. The next transition parameters of the standby systems are
 672 sampled, and the simulation is moved to the earliest transition
 673 time, t . Components with next transition time equal to t are
 674 identified, the required transitions effected, their next transition
 675 times sampled, the new system performance computed, and the
 676 next simulation time determined. This cycle of events continues
 677 until offsite power is recovered. 678

Let μ_{old} hold the node capacities at the previous system transi-
 679 tion, τ , the vector of next node transition times, N , the number
 680 of simulation samples, and $\mathbf{S} = \{s_j\}^N$, the register indicating
 681 the occurrence of an SBO. The indicator register, \mathbf{S} , is such that,
 682 $s_j = 1$ if an SBO occurs in the j th sample, and 0, otherwise.
 683 The simulation algorithm is summarized thus. 684

- 685 i) Initialize the register storing the flow through the out-
 686 put node, set $N = 1$, $\mathbf{S} = \{\}$, and define the simulation
 687 stopping criterion. The stopping criterion could be the
 688 number of LOOP, number of SBO, or convergence of
 689 the SBO probability.
- 690 ii) Determine which component will be unavailable due to
 691 test or maintenance.
- 692 iii) Set $s_N = 0$ and $\tau = \{\infty\}^M$, where M is the number of
 693 nodes in the system.
- 694 iv) Force LOOP as described earlier, accounting for inter-
 695 dependencies according to the procedures described
 696 in Sections II-C1 and II-C2. Remember to sample the
 697 next transition parameters after every node transition
 698 and update τ . See [22] for the procedure for sampling
 699 the transition parameters of a multistate node.
- 700 v) Define μ using the current states of the nodes, that is,
 701 $\mu = \{c_{x_0}^{\{i\}}\}_{M \times 1}$ and set $t = 0$, $\mu_{\text{old}} = \mu$.
- 702 vi) Determine $X_{\text{out}} | X_{\text{out}} = (\mathbf{Y}, \mathbf{t})$ and save as a function
 703 of time.

- 704 vii) Set $s_N = s_N + 1$ if $X_{\text{out}} = 0$ and determine the next
705 simulation time, $t = \min(\tau)$.
- 706 viii) Find nodes with next transition time equal to t . For
707 each node, force the required transition, sample its next
708 transition parameters (except for nodes returning to cold
709 standby), and update μ and τ .
- 710 ix) Restart nodes returning from repairs if X_{out} , as previ-
711 ously determined, is less than 1.
- 712 x) If $\mu_{\text{old}} \neq \mu$;
- 713 a) Compute X_{out} and set $s_N = s_N + 1$ if $X_{\text{out}} = 0$.
714 b) Save X_{out} if different from the previous.
- 715 c) Temporarily set the capacity of the switchyard
716 node to 1 if it is in ‘‘Shutdown’’ and calculate the
717 new system flow. If this flow is nonzero, set the
718 switchyard to start-up, sample its next transition
719 parameters, and update τ .
- 720 xi) Set $\mu_{\text{old}} = \mu$, $t = \min(\tau)$, and check if offsite power
721 is recovered.
- 722 xii) Repeat steps (viii) to (xi) until offsite power is recovered.
723 Discard history N if $s_N = 0$ and set $N = N + 1$.
- 724 xiii) Repeat steps (ii) to (xii) until the simulation stopping
725 criterion is met, and terminate algorithm.
- 726 xiv) Compute the relevant SBO indices

727 A. SBO Indices: Computation and Relevance

728 The SBO frequency, f_s , makes the list of the most informative
729 and desired SBO indices. It defines the expected number of
730 times, per year, an SBO occurs at a plant. If p_1 defines the
731 conditional probability of an SBO given a LOOP occurring at
732 frequency, f_l , per year, then

$$733 \quad f_s = p_1 f_l$$

$$734 \quad p_1 = \frac{\sum (\mathbf{S} > 0)}{N - 1}. \quad (14)$$

735 The fraction of f_s occurring at start-up is deduced from the
736 number of SBO at time 0. This index could be used to assess the
737 efficiency of the start-up procedure, as well as the vulnerability
738 of the generators in cold standby.

739 The nonrecovery probability, $r_1(t)$, defines the likelihood of
740 recovery duration from an SBO accident exceeding a given time.
741 It is computed as detailed in [26], and like p_1 , belongs to the set
742 of inputs to the SBO event tree. Given it defines the unavailabil-
743 ity of power at the plant, $r_1(t)$ can be directly compared with
744 the reliability of the SBO mitigating mechanism. The outcome
745 of such a comparison would help ascertain the adequacy of the
746 mitigating mechanism. In addition, $f_s \times r_1(t)$ yields the fre-
747 quency of exceedance, a measure of the overall SBO risk at the
748 plant. The quantity also presents a means of assessing the rela-
749 tive effectiveness of multiple recovery responses or operational
750 constraints.

751 Finally, the conditional probability of a second SBO, p_2 , given
752 an SBO has already occurred is given by

$$753 \quad p_2 = \frac{\sum (\mathbf{S} > 1)}{\sum (\mathbf{S} > 0)}. \quad (15)$$

754 Knowledge of p_2 may shape the recovery response on the oc-
755 currence of a second SBO. For instance, a plant with a large p_2
756 would require the logistics used in the recovery of the first SBO
757 left in the field and the operations staff kept on high alert. This
758 reduces human error, ensuring a lower nonrecovery probability,
759 $r_2(t)$, of the second SBO.

760 Generally, the conditional probability, p_n , of the n th SBO
761 given the $(n - 1)$ th SBO is expressed as

$$762 \quad p_n = \frac{\sum (\mathbf{S} > n - 1)}{\sum (\mathbf{S} > n - 2)}. \quad (16)$$

763 If absolute probabilities are required instead, the denominator
764 in (16) is replaced with $N - 1$.

765 B. Incorporation Into the Existing Framework

766 Shown in Fig. 5 is an excerpt from the SBO event tree pre-
767 sented in [1]. Of its 12 headings, only four T(PG), EM, ER1,
768 and ER2 are of relevance to SBO recovery. The first depicts
769 LOOP, and requires the LOOP frequency. The second repre-
770 sents SBO occurrence, and requires the unavailability of the
771 standby power systems. Here, the chain of complicated fault
772 trees in the existing model can be replaced with the conditional
773 SBO probability, p_1 . The last two headings represent offsite and
774 standby power recovery, respectively. These can be merged into
775 one heading, say ac power recovery, and the complicated fault
776 trees replaced with a crisp value read from $r_1(t)$. With these, the
777 core damage frequency induced by the first SBO is computed by
778 solving the event tree, using standard procedure. For the second
779 SBO, the first is regarded the initiating event. The LOOP fre-
780 quency, therefore, is replaced with f_s , p_1 with p_2 , and $r_1(t)$
781 with $r_2(t)$.

782 IV. CASE STUDY: AN APPLICATION TO THE MAANSHAN 783 NUCLEAR POWER PLANT IN TAIWAN

784 The Maanshan plant is a two-unit, 1902 MW, Westinghouse
785 PWR nuclear power plant operated by the Taiwan Power Com-
786 pany. Its offsite power is supplied by six independent sources,
787 four of which are connected to the 345-kV switchyard and the re-
788 mainder, through the 161-kV switchyard. It is powered through
789 two safety buses, AIE-PB-S01 and BIE-PB-S01, each with a
790 dedicated EDG: DG-A, and DG-B, respectively. A shared EDG,
791 DG-5, connected as shown in Fig. 6 is available as a backup in
792 case any of the dedicated generators is unavailable. In addition
793 to the shared EDGs, are two GTGs, GT1 and GT2, connected
794 via the 161-kV switchyard. These generators form the alterna-
795 tive emergency power system of the plant, each satisfying the
796 demand on both power trains.

797 During normal plant operation, the safety buses are fed by
798 the main plant generator, G1, via the red lines and the normally
799 closed breakers 19 and 01. On plant shut down, G1 becomes
800 unavailable, and the safety buses are forced to tap power from
801 the 345-kV switchyard (via the blue lines and the normally
802 open breakers 17 and 03) or the 161-kV switchyard (via the
803 green lines and the normally open breakers 15 and 05). When
804 these sources also become unavailable, DG-A and DG-B are
805 automatically started and aligned. DG-5 is manually started and

LOOP	ONSITE POWER FAILURE	REACTOR PROTECTION SYSTEM	RCS	AFW	EMERGENCY DEPRESURIZATI	RCP SEAL ONSTAGE 1 INTEGRITY	RCP SEAL STAGE 1 INTEGRITY	RCP SEAL STAGE 2 INTEGRITY	RCP SEAL STAGE 2 INTEGRITY	OFFSITE POWER RECOVERY	ONSITE POWER RECOVERY
T(PG)	EM	K	Q	L(T)	X(E)	BP1	O1	BP2	O2	ER1	ER2

Fig. 5. Excerpt from the SBO event tree showing headings (credit: [1]).

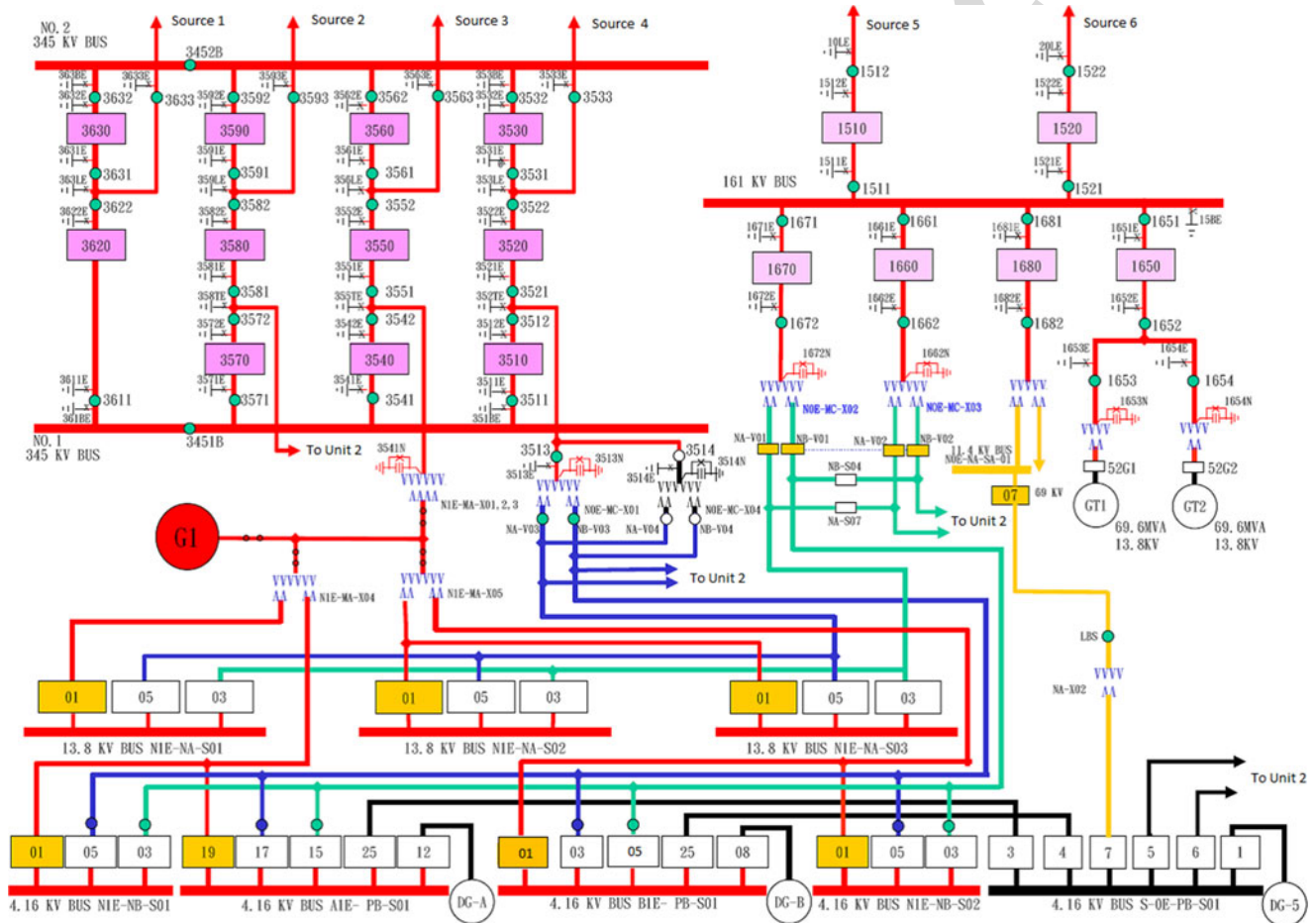


Fig. 6. Layout of the Maanshan nuclear power plant ac distribution system (credit: Dr. S.-K. Chen, NTHU, Taiwan).

802 aligned by the plant operators on the failure of any of these. The
 803 manual start-up and alignment procedure of GT1 and GT2
 804 is initiated when at least 2 out of the 3 EDGs become unavailable.
 805 Following their successful start-up, the GTGs take about 30 min
 806 to become fully functional.

807 A probabilistic assessment of the SBO risk of the plant due
 808 to grid and switchyard initiated LOOP is required.

809 A. Developing the System and Component Models

810 Fig. 7 is the simplified schematic of the plant's ac power
 811 system, showing all the elements relevant to an SBO. DG-5,
 812 though serving only one bus at a time, is assumed connected to
 813 both buses in the system's adjacency matrix. This implies, its
 814 flow is divided between the buses, contrary to what is obtained
 815 in reality. However, since the flows from the two buses are

emptied into the virtual output node, t , the total flow from the
 shared generator is accounted for. As shown, the six grid sources
 and the two switchyard sources have each been represented by
 single nodes, as proposed in Section II-B1.

Nodes 1, 7, 8, and 9 are modeled as proposed in Sections II-B
 and II-B1. The switchyard, on the other hand, is modeled according
 to Fig. 3, to account for human error during its start-up from
 shut down. Since DG-A (node 5) and DG-B (node 6) are
 automatically started following a LOOP, they are not susceptible
 to human error, and, therefore, are modeled as shown in Fig. 8.
 DG-5, GT1, and GT2, however, require human intervention for
 their start-up and alignment. Node 10, therefore, is modeled
 according to Fig. 9 and nodes 3 and 4, according to Fig. 10.

Justifying the values assigned to the state capacities of the
 generators, recall the system consists of 2 safety buses ($m = 2$)
 with each of DG-A and DG-B serving only one bus at a time

816
817
818
819
820
821
822
823
824
825
826
827
828
829
830
831

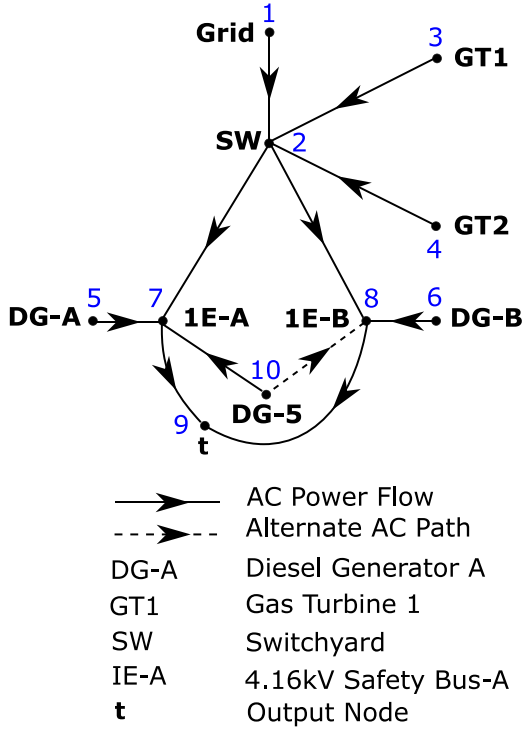


Fig. 7. Simplified schematic of plant's ac distribution system.

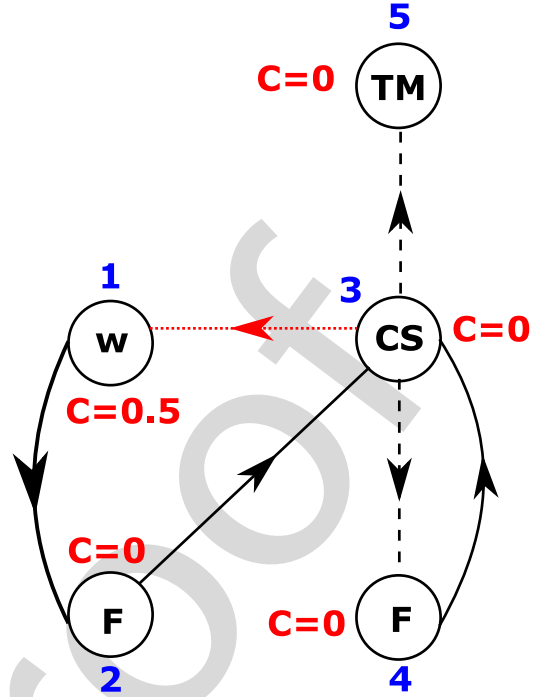


Fig. 8. Multistate model for the main diesel generators (DG-A and DG-B).

832 ($n_1 = 1$). Since these generators can, however, fully meet the de-
 833 mand on the bus they serve ($u = 1$), they are assigned a capacity
 834 of 0.5 when working, as proposed in Section II-B. The GTs,
 835 on the other hand, can fully serve both buses simultaneously
 836 ($n_1 = 2$), and therefore, have a capacity of 1 when working.
 837 From the multistate models, the capacity vector for the main
 838 diesel generators, the shared diesel generator, and the GTs are
 839 $\{0.5, 0, 0, 0, 0\}$, $\{0.5, 0, 0, 0, 0, 0, 0\}$, and $\{1, 0, 0, 0, 0, 0, 0\}$,
 840 respectively. Using these parameters in conjunction with Fig. 7,
 841 the adjacency matrix of the system is derived as

$$A = \begin{pmatrix} 0 & 1 & 0 & 0 & 0 & 0 & 0 & 0 & 0 & 0 \\ 0 & 0 & 0 & 0 & 0 & 0 & 1 & 1 & 0 & 0 \\ 0 & 1 & 0 & 0 & 0 & 0 & 0 & 0 & 0 & 0 \\ 0 & 1 & 0 & 0 & 0 & 0 & 0 & 0 & 0 & 0 \\ 0 & 0 & 0 & 0 & 0 & 0 & 1 & 0 & 0 & 0 \\ 0 & 0 & 0 & 0 & 0 & 0 & 0 & 1 & 0 & 0 \\ 0 & 0 & 0 & 0 & 0 & 0 & 0 & 0 & 1 & 0 \\ 0 & 0 & 0 & 0 & 0 & 0 & 0 & 0 & 0 & 1 \\ 0 & 0 & 0 & 0 & 0 & 0 & 0 & 0 & 0 & 0 \\ 0 & 0 & 0 & 0 & 0 & 0 & 1 & 1 & 0 & 0 \end{pmatrix}$$

842 Given the adjacency matrix, the other parameters of the system
 843 flow equations are obtained as described in Section II-A, where
 844 $s = \{1, 3, 4, 5, 6, 10\}$ and $t = 9$. Fig. 11 is the system's graph
 845 model showing the maximum flow along each link, derived from
 846 the adjacency matrix and the maximum node capacities.

847 *Component Reliability Data:* Though realistic, the data used
 848 do not represent the actual data for the Maanshan plant. They
 849 were, however, assumed with the view to reflecting the reliability

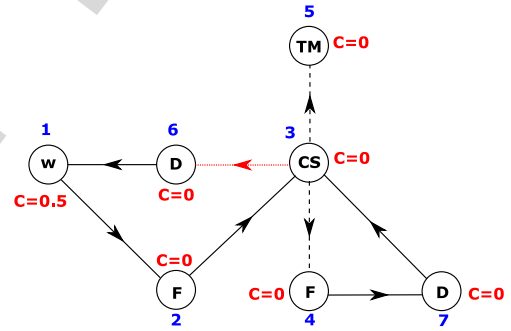


Fig. 9. Multistate model for the shared diesel generator (DG-5).

850 data used in Volumes 1 and 2 of the NUREG/CR-6890 report
 851 (see [1] and [2]).

852 The repair times for the six grid sources are lognor-
 853 mally distributed with means and corresponding standard de-
 854 viations defined by $\{8.99, 11.84, 8.24, 10.25, 9.61, 9.15\}$ and
 855 $\{6.71, 4.83, 4.05, 6.61, 1.92, 5\}$, respectively. Similarly, switch-
 856 yard repair times are lognormally distributed, with $\{8, 10.41\}$
 857 and $\{5.83, 2.5\}$, respectively, being the sets of means and cor-
 858 responding standard deviations for the two switchyards. The
 859 effective repair distributions for the grid and switchyard nodes
 860 are modeled according to the proposal in Section II-B1, as shown
 861 in Figs. 12 and 13, respectively.

862 All five standby generators are assumed to have a start-up
 863 failure probability of 1.756×10^{-2} . Also, the human errors as-
 864 sociated with the failure to complete the start-up procedures
 865 for GT-5 and the switchyard are assumed equal but one-sixth
 866 of those for GT1 and GT2. Table I defines the probability of

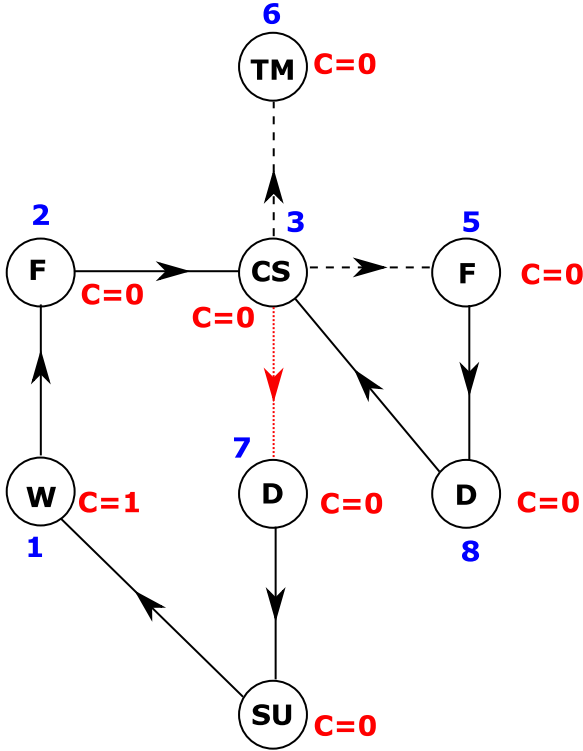


Fig. 10. Multistate model for the GTGs (GT1 and GT2).

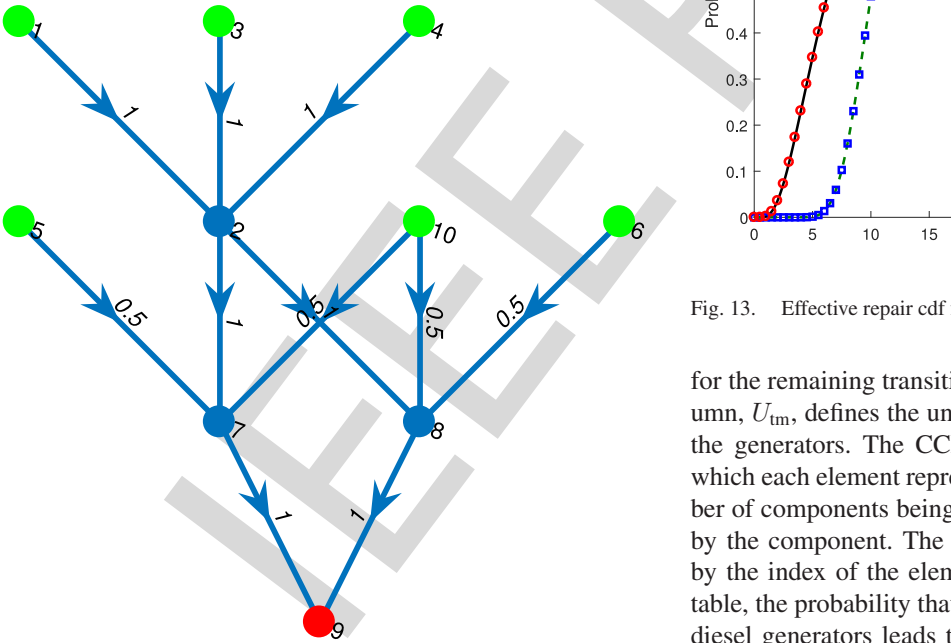


Fig. 11. Full system graph model showing maximum flow along links.

867 the operators not completing the start-up of the GTGs within
 868 selected times. Using the procedure proposed in Section II-B3,
 869 the parameters defining transitions $7 \rightarrow 4$ and $5 \rightarrow 8$ of the
 870 GTGs were obtained. The same procedure was used to obtain
 871 the parameters for transitions $6 \rightarrow 1$ and $4 \rightarrow 7$ of DG-5 and
 872 transition $4 \rightarrow 1$ of the switchyard. These and the parameters

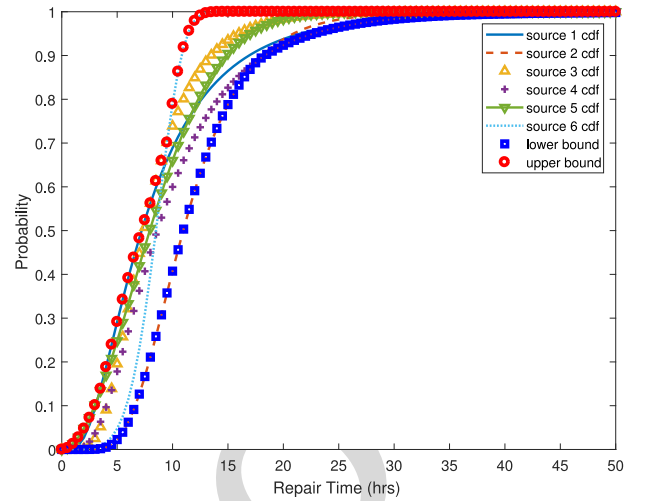


Fig. 12. Effective repair cdf for multiple grid sources.

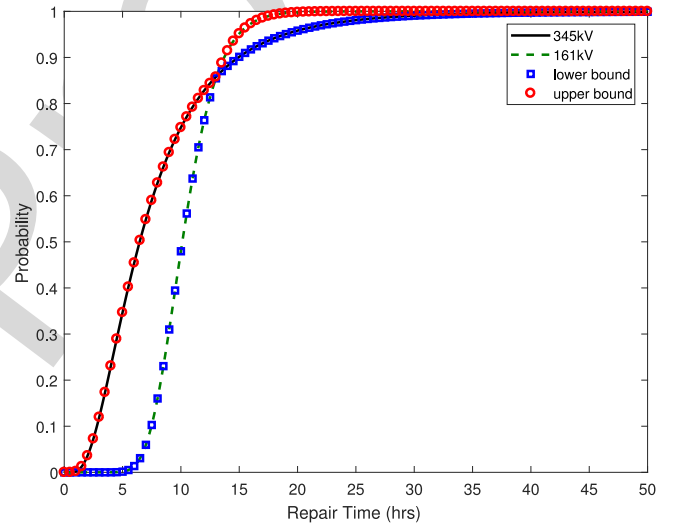


Fig. 13. Effective repair cdf for multiple switchyard nodes.

for the remaining transitions are presented in Table II. The column, U_{tm} , defines the unavailability due to test/maintenance of the generators. The CCF parameters are defined by a set in which each element represents the probability of a certain number of components being involved in any failure event initiated by the component. The number of components is determined by the index of the element in the set. For instance, from the table, the probability that the start-up failure of any of the main diesel generators leads to the failure of the other generator is 0.021. This implies a total of two component failures, explaining why the probability value is the second element of the set (see Section II-C1 for details). Transition $4 \rightarrow 1$ of the GTGs depicts their start-up duration, which as we are told in Section IV, takes 30 min, explaining why it is assigned a deterministic 0.5 h.

B. Representing Component Interdependencies

The first and easily recognizable form of interdependency in the system is CCF, where the failure of a generator could trigger

TABLE I
HUMAN ERROR PROBABILITIES FOR GT1 AND GT2

Time (h)	1	2	3	4	6	7	8	10
Probability	2.07×10^{-1}	2.07×10^{-2}	3×10^{-3}	3×10^{-4}	2×10^{-4}	1×10^{-4}	1×10^{-5}	1×10^{-5}

TABLE II
COMPONENT RELIABILITY DATA

Component	Transition	Distribution		U_{tm}	CCF Parameters	
		Type	Parameters		Start-up Failure	Running Failure
DG-A & DG-B	1-2	Weibull	(100,1.24)	0.009	{0.979, 0.021}	{0.972, 0.028}
	2-3	Lognormal	(6.42,2)			
	4-3	Lognormal	(5,1.2)			
GT1 >2	4-1	deterministic	0.5	0.0099	{0.959, 0.041}	{0.962, 0.038}
	4-2	Weibull	(200,1.5)			
	2-3	Lognormal	(5,2)			
	8-3	Lognormal	(7,1.8)			
	1-2	Weibull	(100,1.05)			
	7-4	Weibull	(0.2872,0.8194)			
	5-8	Weibull	(0.2872,0.8194)			
DG-5	1-2	Weibull	(100,1.24)			
	2-3	Lognormal	(6.42,2)			
	7-3	Lognormal	(5,1.2)			
	6-1	Weibull	(0.197,0.7467)			
	4-7	Weibull	(0.197,0.7467)			
Switchyard	4-1	Weibull	(0.197,0.7467)			
	2-1	See Fig. 13				
Grid	2-1	See Fig. 12				

TABLE III
CCG DEFINITION

CCG	Description	Attributes	
		Designation	Value
1	Emergency Diesel Generator failure to start	ρ	{5, 6}
		θ	{0.979, 0.021}
		β_1	4
		β_2	3
2	Emergency Diesel Generator failure to run	ρ	{5, 6}
		θ	{0.972, 0.028}
		β_1	2
		β_2	1
3	Gas Turbine Generator failure to start	ρ	{3, 4}
		θ	{0.959, 0.041}
		β_1	4
		β_2	3
4	Gas Turbine Generator failure to run	ρ	{3, 4}
		θ	{0.962, 0.038}
		β_1	2
		β_2	{1, 4}

890 the almost instantaneous failure of another generator. This type
 891 of interdependency is modeled according to the CCF model
 892 presented in Section II-C1. DG-A and DG-B, as we know, are
 893 of the same design and model, different from the make of DG-
 894 5. Therefore, while the former are susceptible to CCF, DG-5
 895 is immune. Similarly, GT1 and GT2 are susceptible to CCF,
 896 giving rise to four CCGs, as defined in Table III. The table is
 897 developed from the CCF parameters in Table II in conjunction
 898 with the CCF model proposed in Section II-C1. CCG 1, for
 899 instance, represents the CCF due to the start-up failure of any of
 900 the main diesel generators. Since these generators are denoted
 901 as nodes 5 and 6 in the system, ρ , the set of components in the
 902 CCG is defined as {5, 6}. Now, as shown in Fig. 8, the start-up

failure of DG-A or DG-B is denoted by state 4. Also, the other
 generator could only be affected by this event if it is in cold
 standby (state 3) at the time of occurrence. This explains why
 β_1 and β_2 are assigned the values, 4 and 3, respectively. The
 parameters for CCG 2 to 4 are derived in a similar fashion.

The other form of interdependency, like the grid failure nec-
 cessitating the start-up of the standby generators or the failure
 of GT-5 forcing the start-up of the GTGs, is a little more sub-
 tle and difficult to deduce. It requires a good knowledge of the
 operating principle of the system and cannot be modeled by
 the CCF model. For this, the cascading failure model proposed
 in Section II-C2 is invoked. To ensure the reproducibility of
 the case study, the step-by-step procedure for developing the

916 dependency matrices have been shown by recreating the se-
917 quence of events following a LOOP.

918 1) Let us assume the occurrence of the initiating event
919 (LOOP), due to the failure of the grid (node 1). As
920 already stated at the beginning of Section IV, the main
921 diesel generators, A (node 5) and B (node 6), are restarted
922 from cold standby. This is accounted for by the first two
923 rows of the dependency matrix, \mathbf{D}_1 . However, if the main
924 generators are not in cold standby, maybe

$$\begin{aligned} \mathbf{D}_1 = \mathbf{D}_2 &= \begin{pmatrix} 2 & 5 & 3 & 1 \\ 2 & 6 & 3 & 1 \\ 2 & 5 & -3 & -3 \\ 2 & 6 & -3 & -3 \end{pmatrix} \\ \mathbf{D}'_5 = \mathbf{D}'_6 &= \begin{pmatrix} -3 & 10 & 3 & 6 \\ -3 & 10 & -3 & -3 \end{pmatrix} \\ \mathbf{D}'_{10} &= \begin{pmatrix} -3 & 3 & 3 & 7 \\ -3 & 4 & 3 & 7 \end{pmatrix} \end{aligned} \quad (17)$$

925 due to test/maintenance or failure, the shared standby gen-
926 erator, DG-5 (node 10), is restarted. Recalling the concept
927 of joint dependency discussed in Section II-C2, the joint
928 dependency between the grid and DG-5 can be deduced.
929 Here, the main generators are the intermediate nodes,
930 since they dictate whether or not to start the shared gen-
931 erator. This behavior is jointly represented by the last two
932 rows of \mathbf{D}_1 and the first row of \mathbf{D}'_5 in (17). Again, if the
933 shared generator too is unavailable (i.e., it is not in cold
934 standby), the GTGs, GT1 (node 3) and GT2 (node 4), are
935 restarted (see Fig. 10). This attribute is jointly represented
936 by \mathbf{D}'_{10} and the last row of \mathbf{D}'_5 . If, however, the GTGs
937 are not in cold standby on arrival of their start-up signal,
938 no action is taken. This is due to the fact that the signal
939 signifies the unavailability of all the standby sources at
940 the plant. \mathbf{D}'_5 and \mathbf{D}'_6 are equal because nodes 5 and 6
941 produce the same effect on the shared generator when un-
942 available for start-up. Similarly, \mathbf{D}_1 and \mathbf{D}_2 are equal, as
943 the response of the standby systems is the same for grid
944 and switchyard failures

$$\mathbf{D}_5 = \begin{pmatrix} 2 & 6 & 3 & 1 \\ 4 & 6 & 3 & 1 \\ 2 & 6 & -3 & -3 \\ 4 & 6 & -3 & -3 \end{pmatrix}. \quad (18)$$

945 2) DG-A (node 5) fails to start or starts but fails to run (see
946 Fig. 2). The system will first check if DG-B (node 6) is
947 available for start-up and initiate its start up, if available.
948 This behavior is defined by the first two rows of \mathbf{D}_5 , as
949 shown in (18). The effect of the unavailability of DG-B
950 on arrival of its start-up signal has already been defined in
951 scenario 1) (see the last row of \mathbf{D}_1). This representation is
952 adapted to account for the case when DG-A fails to start
953 or run and DG-B is unavailable for start-up, in the last two

rows of \mathbf{D}_5 [see (18)]

954

$$\mathbf{D}_6 = \begin{pmatrix} 2 & 5 & 3 & 1 \\ 4 & 5 & 3 & 1 \\ 2 & 5 & -3 & -3 \\ 4 & 5 & -3 & -3 \end{pmatrix}. \quad (19)$$

- 3) Similarly, DG-B (node 6) fails to start or starts but fails
955 to run (see Fig. 8). The system will first check if DG-A
956 (node 5) is available, and initiate its start-up. The ensuing
957 sequence of events is similar to that in scenario 2). Hence,
958 the dependency matrix is as obtained in (19). 959
- 4) DG-5 in cold standby fails to start or starts but fails to run
960 (see Fig. 9). In this case, any repaired EDG is restarted
961 first, otherwise, the GTG are restarted. The ensuing possi-
962 ble sequence of events are already covered by scenarios
963 (1)–(3), and it is, therefore, recommended to not explicitly
964 redefine these in \mathbf{D}_{10} , for simplicity. It is deducible that
965 the failure of DG-5 induces the same response sequence as
966 grid or switchyard failure. Therefore, recreating a LOOP
967 event accounts for the failure of DG-5. Hence 968

$$\mathbf{D}_{10} = \begin{pmatrix} 2 & 1 & 2 & 2 \\ 2 & 2 & 2 & 2 \\ 4 & 1 & 2 & 2 \\ 4 & 2 & 2 & 2 \end{pmatrix} \quad \mathbf{D}'_1 = \mathbf{D}_1 \quad \mathbf{D}'_2 = \mathbf{D}_2.$$

- 5) GT1 (node 3) starts up successfully and enters the start-up
969 state (see Fig. 10). Recall, states 7 and 8 account for the
970 time taken by the operator to initiate the start-up of the
971 generator. However, since both GT1 and GT2 (node 4)
972 are in the same location, they are exposed to equal delays.
973 Hence, the transitions, $7 \rightarrow 4$ and $5 \rightarrow 8$, of GT1 and GT2
974 are equal. To ensure the satisfaction of this constraint,
975 when GT1 enters state 4, GT2 too is forced to state 4 if it
976 is in state 7 or state 8, if it is in state 5. Similarly, when
977 GT1 enters state 8, GT2 is forced to state 8 if it is in state
978 5 or state 4 if it is in state 7. This behavior is expressed by
979 the first four rows of \mathbf{D}_3 , as shown in (20). 980
- 6) GT2 (node 4) starts up successfully and enters the start-up
981 state (see Fig. 10). This scenario has the same effect on
982 GT1 (node 3) as scenario (v) has on GT2. Therefore, the
983 ensuing sequence of events is accounted for by the first
984 four rows of \mathbf{D}_4 , as shown in the following: 985

$$\begin{aligned} \mathbf{D}_3 &= \begin{pmatrix} 8 & 4 & 5 & 8 \\ 8 & 4 & 7 & 4 \\ 4 & 4 & 5 & 8 \\ 4 & 4 & 7 & 4 \\ 2 & 4 & 3 & 7 \\ 2 & 4 & 2 & 2 \\ 2 & 4 & 8 & 8 \\ 2 & 4 & 5 & 5 \\ 2 & 4 & 6 & 6 \end{pmatrix} & \mathbf{D}_4 &= \begin{pmatrix} 8 & 3 & 5 & 8 \\ 8 & 3 & 7 & 4 \\ 4 & 3 & 5 & 8 \\ 4 & 3 & 7 & 4 \\ 2 & 3 & 3 & 7 \\ 2 & 3 & 2 & 2 \\ 2 & 3 & 8 & 8 \\ 2 & 3 & 5 & 5 \\ 2 & 3 & 6 & 6 \end{pmatrix} \\ \mathbf{D}'_3 = \mathbf{D}'_4 &= \begin{pmatrix} 2 & 1 & 2 & 2 \\ 5 & 1 & 2 & 2 \\ 6 & 1 & 2 & 2 \\ 8 & 1 & 2 & 2 \end{pmatrix}. \end{aligned} \quad (20)$$

TABLE IV
 SUMMARY OF THE STATIC SBO INDICES OBTAINED

LOOP Type	p_1	f_s (per yr)	p_2	% of SBO at Start-Up	Simulation Samples
Grid	0.0033	6.18×10^{-3}	0.0022	29.23	1×10^8
Switchyard	0.0035	3.65×10^{-3}	0.0153	27.97	4.5×10^7

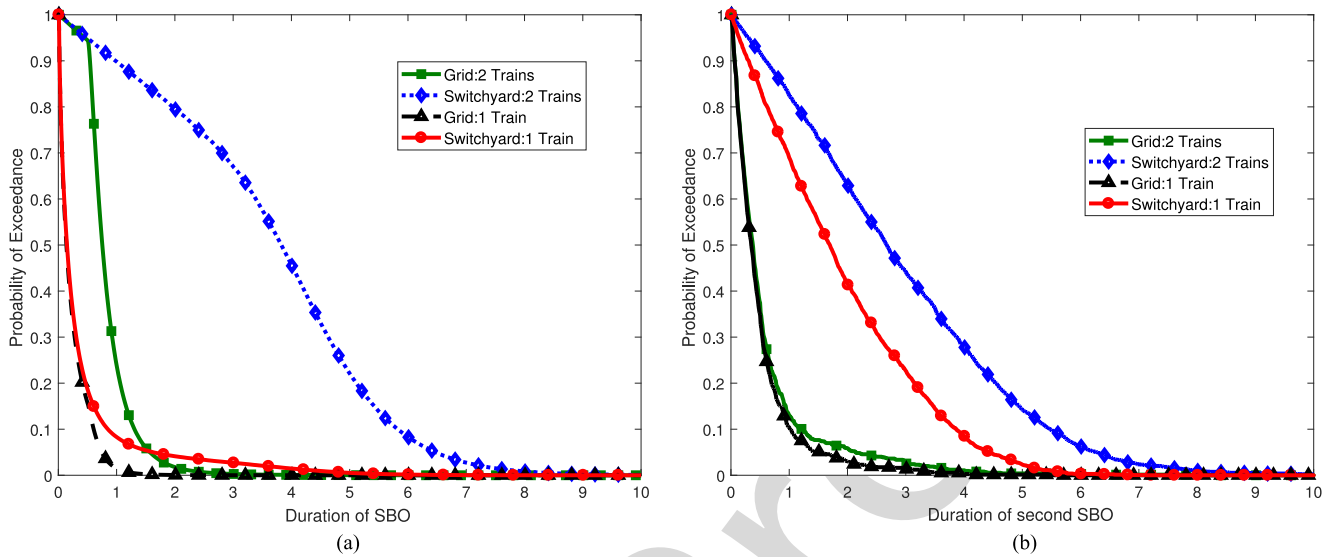


Fig. 14. Probability of SBO duration exceedance.

986 7) GT1 fails to run. GT2 is restarted, if it is available for
 987 start-up, otherwise the system checks whether or not the
 988 failed diesel generators have been repaired. The first case
 989 is represented by the fifth row of D_3 , as shown in (20).
 990 The sequence of events involved in the second case is similar
 991 to the events following a LOOP. Therefore, a LOOP scenario
 992 is recreated, as shown in the last four rows of D_3 and D'_4 .
 993 States 1, 4, and 7 have been left out of the possible GT2
 994 states to necessitate the second case because, they mean
 995 either GT2 is already in operation (state 1), or on the verge
 996 of operation (states 4 and 7).
 997 8) Similarly, GT2 failure to run produces the same effect
 998 on GT1 and the diesel generators, as in scenario (7). The
 999 ensuing sequence of events is defined by D_4 and D'_3 .

1000 We have not considered the sequence of events following
 1001 the failure of the GTGs to start because, being the last standby
 1002 sources to be called into operation, their start-up failure means
 1003 the unavailability of the other standby sources.

1004 C. Results and Discussions

1005 The proposed framework is implemented in the open source
 1006 uncertainty quantification toolbox, OpenCOSSAN [27], [28],
 1007 and used to quantify the SBO risk at the Maanshan nuclear
 1008 power plant. For a grid and switchyard LOOP frequency of
 1009 1.86×10^{-2} and 1.04×10^{-2} per/year respectively, the case
 1010 study was analyzed on a 2.5-GHz, E5-2670 v2 Intel Xeon CPU.
 1011 A 5% coefficient of variation was imposed on the conditional
 1012 probability of SBO as the simulation convergence criterion. The
 1013 analysis took about 3 h, and the results yielded are summarized

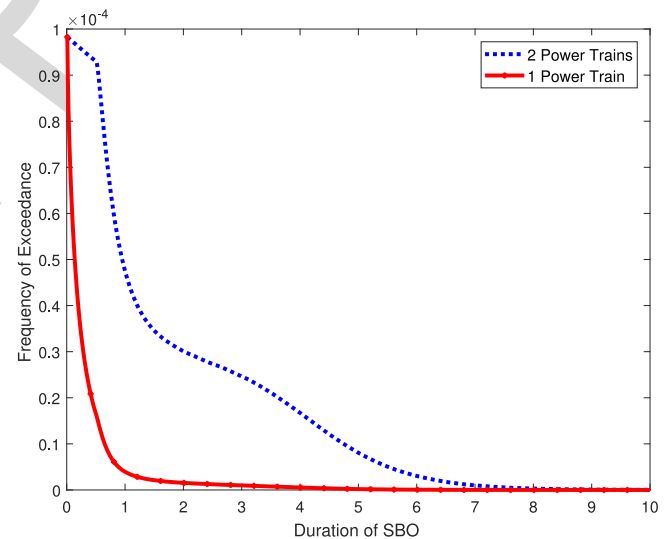


Fig. 15. Composite frequency of first SBO exceedance.

1014 in Table IV, Fig. 14, and Fig. 15. The probability of exceedance
 1015 gives a measure of the likelihood of nonrecovery from the SBO
 1016 within a given time. The composite frequency of exceedance is
 1017 the sum of the frequencies of exceedance yielded by the two
 1018 LOOP categories.

1019 As shown in Table IV, the probability of an SBO given a
 1020 LOOP is almost the same for both LOOP categories. The slight
 1021 difference is due to the fact that the GTG is unusable during
 1022 switchyard centred LOOP. Their effect, however, is prominent in

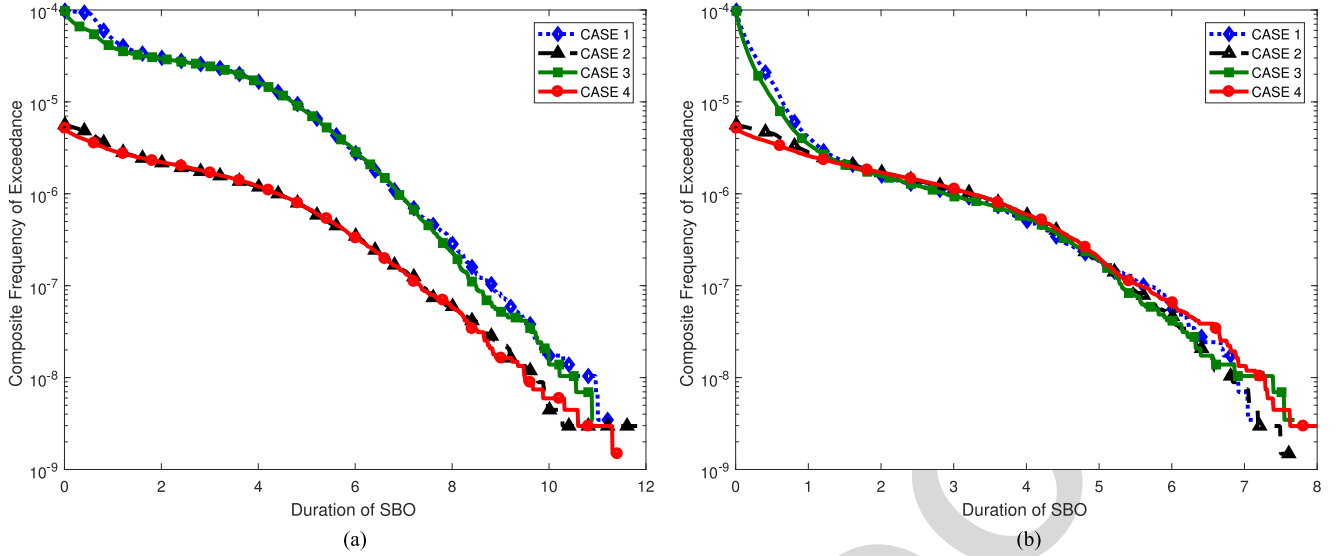


Fig. 16. Comparison of composite frequencies of exceedance. (a) Composite frequencies of exceedance when a minimum of two powertrains are required for power recovery; (b) Composite frequencies of exceedance when one power train is sufficient for power recovery.

1023 mitigating the second SBO. The nonrecovery probability from
 1024 an SBO, as shown in Fig 14, is expressed as the nonrecovery
 1025 likelihood as a function of time and number of safety buses.
 1026 The overall SBO risk at the plant is defined by the composite
 1027 frequency of exceedance, as shown in Fig. 15.

1028 As a way of verifying the convergence of the simulation,
 1029 the product of p_1 and the fraction of SBO at start-up, should
 1030 match the probability, p_0 , of the emergency power system be-
 1031 ing unavailable at time 0. Bear in mind that GT-5 and the GTG
 1032 have no influence on p_0 , as a result of the delays characteriz-
 1033 ing their start-up. Therefore, the emergency power system is
 1034 unavailable at start-up only if DG-A (or DG-B) is unavailable
 1035 due to test/maintenance and DG-B (or DG-A) fails to start or
 1036 both are not in test/maintenance but fail to start. If U_{tm} is the
 1037 unavailability due to test/maintenance of DG-A and DG-B and
 1038 p_s , their start-up failure probability, p_0 is obtained as

$$p_0 = U_{tm}(p_s + p_s) + (1 - U_a)p_s^2$$

$$p_0 = 2U_{tm}p_s + (1 - U_{tm})p_s^2. \quad (21)$$

1039 Substituting the required values in (21), an error of 3.17% is
 1040 realized for grid LOOP and 4.7%, for switchyard LOOP. Since
 1041 the error in each case is not in excess of 5%, the convergence of
 1042 the simulation is verified.

1043 Ensuring an enhanced risk insight, the system was reanalyzed
 1044 for three additional scenarios as follows.

- 1045 1) *Case 2*: No delays in the start-up of DG-5. This implies,
 1046 the effects of human error are removed.
- 1047 2) *Case 3*: GTG start-up is simultaneous with DG-A and
 1048 DG-B. The generators, however, are kept in warm standby
 1049 after start-up.
- 1050 3) *Case 4*: A combination of Case 2 and Case 3.

1051 Case 1 represents the scenario already analyzed, and the
 1052 results for the four cases are summarized in Figs. 16 to 18
 1053 (please note the composite frequencies in Figs. 16(a) and (b) are

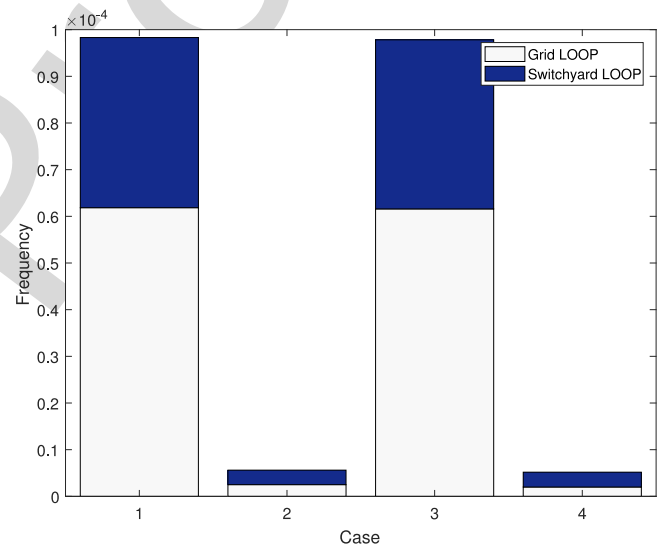


Fig. 17. Comparison of SBO frequencies.

expressed on a log-scale). We have used absolute, instead of
 1054 conditional probabilities in Fig. 18, to ensure uniformity. 1055

The following risk insights are inferred by the outcome of the
 1056 case study. 1057

- 1) As shown in Fig. 14, SBOs induced by switchyard fail-
 1058 ures are more difficult to recover from and, therefore, con-
 1059 tribute more to the overall SBO risk at the plant. In this
 1060 light, feasible reliability improvement programs should be
 1061 designed to ensure the high reliability of the switchyard. 1062
 Such a reliability program should be complemented by an
 1063 efficient repair policy to keep the nonrecovery probability
 1064 low. 1065
- 2) The GTGs are the only difference between the recovery
 1066 durations of grid and switchyard LOOP. These generators,
 1067 therefore, are very instrumental to mitigating SBO risks
 1068 at the plant, and their availability should be kept high. 1069

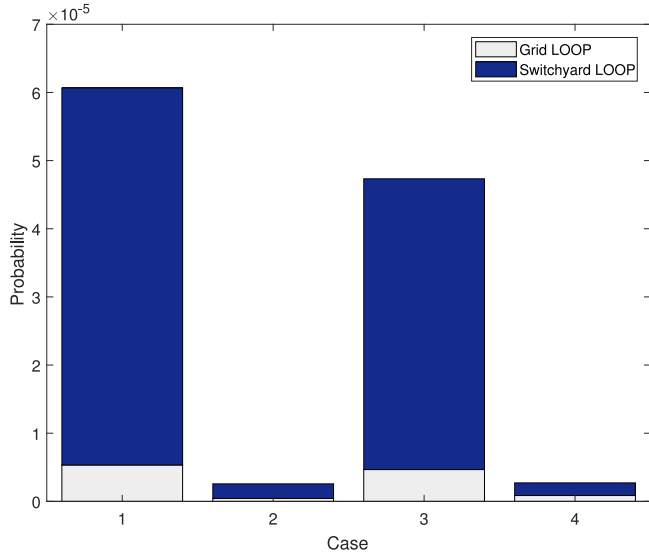


Fig. 18. Comparison of second SBO probabilities.

3) Automating the start-up of DG-5 and initiating the start-up of the GTG just after LOOP guarantees an improved resilience to SBO, as endorsed by Figs. 16 to 18. However, starting the GTG simultaneously with the EDG brings with it additional costs, borne from fuel consumption and maintenance. This decision, therefore, should be preceded by a robust cost-benefit analysis. In fact, under economic constraints, it is prudent to automate the start-up of DG-5 only, as the difference between the outcomes yielded by Case 2 and Case 4 is only just slight.

In this case study, we have ignored the explicit sensitivity and importance analyses of the individual components, since these quantities can be achieved even with the existing techniques.

V. CONCLUSION

SBO accidents, though a rare occurrence, can have devastating consequences on a nuclear power plant's ability to achieve and maintain safe shut down. Consequently, the plant's capability to cope and recover from such occurrences makes a key input to its probabilistic risk assessment model.

In this paper, we have proposed an intuitive simulation framework to model a nuclear power plant's recovery from SBO accidents. The framework provides a simple means of defining the complex interdependencies that often characterize the operation of practical engineering systems, and therefore, applicable without unrealistic assumptions. This attribute, coupled with its ability to intuitively tolerate the multistate behavior of the system's building block, distinguishes it from the existing approaches. Its applicability has been demonstrated by modeling the SBO recovery of a pressurized water reactor, providing an informed insight into its SBO risks. The proposed approach was able to fully model the dynamic behavior of the power system and provide valuable insights on the SBO risk at the plant. The nonrecovery probability curve obtained, for instance, can be absorbed into the existing probabilistic risk assessment models,

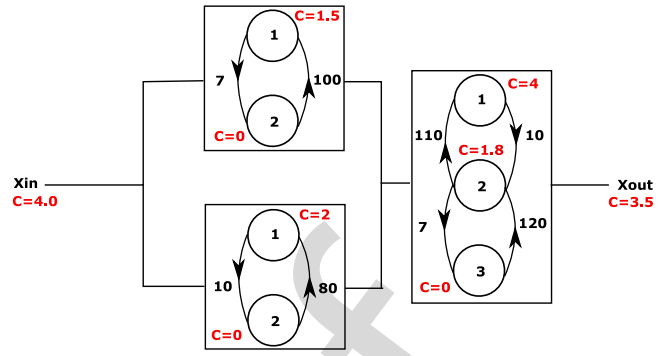


Fig. 19. Structure of a three-component pipe network.

getting rid of laborious fault trees. Since this curve also depicts the unavailability of ac power, it can be directly compared with the reliability of the plant's SBO coping mechanism, providing an easier means of determining the need for their reliability improvement. It also helps ascertain the adequacy of the plant's SBO recovery capability, without revisiting the entire model. A key desirable feature of the proposed framework is its wide applicability, even to nonnuclear applications.

In spite of their well-documented limitations relative to the proposed framework, the existing static fault tree-based models still possess desirable attributes that give them an edge in importance, sensitivity, and uncertainty analyses. With this in mind, the proposed framework has been developed with the view to complementing their applicability, instead of serving as an explicit replacement. We have, therefore, included a clear description of how its output can be incorporated into these models. The framework, in addition, has been implemented in the open-source uncertainty quantification toolbox developed at the Institute for Risk and Uncertainty (see [27] and [28]), thereby rendering it readily available.

The multistate model and dependency matrices proposed create the foundation for the incorporation of additional dynamic considerations. Such considerations as the optimal number of maintenance teams on-site, EDG failure during cold standby, optimal inspection interval, and the availability of spares are a possibility. Efforts are underway to extend the framework to these considerations, other LOOP categories, and incorporate epistemic uncertainties.

APPENDIX

This section is introduced with the view to providing a detailed example of how the linear programming problem is formulated, stating the exact values of the relevant parameters. The goal is to enable readers to grasp, fully, the concept proposed in this paper, as well as provide a benchmark for validating their implementation of this concept.

Consider the three-component pipeline shown in Fig. 19, adapted from [22]. A maximum of four tons of oil could be pumped from the source, X_{in} , to the output, X_{out} , where the demand is fixed at 3.5 tons. The state-space of each of the other components is shown, with the number beside each

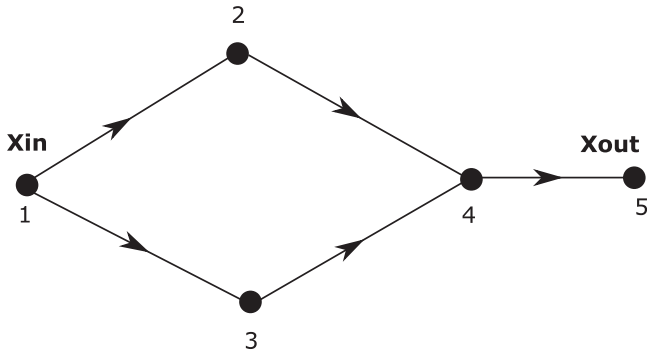


Fig. 20. Network model of pipe network.

1144 state denoting the capacity of the component in that state. The
 1145 equivalent graph model of the system is shown in Fig. 20. Notice
 1146 the two extra nodes, 1 and 5, representing the source and output,
 1147 respectively. The available information is sufficient to formulate
 1148 the linear programming problem and derive its parameters. The
 1149 first step is to define the adjacency matrix, since all the other
 1150 parameters depend on it. From Fig. 20, the adjacency matrix,
 1151 \mathbf{A} , is obtained as

$$\mathbf{A} = \begin{pmatrix} 0 & 1 & 1 & 0 & 0 \\ 0 & 0 & 0 & 1 & 0 \\ 0 & 0 & 0 & 1 & 0 \\ 0 & 0 & 0 & 0 & 1 \\ 0 & 0 & 0 & 0 & 0 \end{pmatrix}.$$

1152 The next task is to deduce the edge and incidence matrices, \mathbf{e}
 1153 and $\mathbf{\Gamma}$, respectively. They are obtained thus

$$\mathbf{e} = \begin{pmatrix} 1 & 2 \\ 1 & 3 \\ 2 & 4 \\ 3 & 4 \\ 4 & 5 \end{pmatrix} \quad \mathbf{\Gamma} = \begin{pmatrix} 1 & 1 & 0 & 0 & 0 \\ -1 & 0 & 1 & 0 & 0 \\ 0 & -1 & 0 & 1 & 0 \\ 0 & 0 & -1 & -1 & 1 \\ 0 & 0 & 0 & 0 & -1 \end{pmatrix}.$$

1154 With \mathbf{A} , \mathbf{e} , and $\mathbf{\Gamma}$ known, the linear programming problem is
 1155 formulated as follows.

1156 1) At time 0, all the components are in their best performance
 1157 state. The inequality constraint, therefore, is expressed as

$$\begin{pmatrix} 1 & 1 & 0 & 0 & 0 \\ 1 & 0 & 0 & 0 & 0 \\ 0 & 1 & 0 & 0 & 0 \\ 0 & 0 & 1 & 1 & 0 \\ 0 & 0 & 0 & 0 & 1 \end{pmatrix} \begin{pmatrix} X_{12} \\ X_{13} \\ X_{24} \\ X_{34} \\ X_{45} \end{pmatrix} \leq \begin{pmatrix} 4.0 \\ 1.5 \\ 2 \\ 4 \\ 3.5 \end{pmatrix}.$$

1158 2) The equality constraint is expressed as

$$\begin{pmatrix} -1 & 0 & 1 & 0 & 0 \\ 0 & -1 & 0 & 1 & 0 \\ 0 & 0 & -1 & -1 & 1 \end{pmatrix} \begin{pmatrix} X_{12} \\ X_{13} \\ X_{24} \\ X_{34} \\ X_{45} \end{pmatrix} = \begin{pmatrix} 0 \\ 0 \\ 0 \end{pmatrix}.$$

3) The bounds on the flow through the edges are

1159

$$\mathbf{lb} = \begin{pmatrix} 0 \\ 0 \\ 0 \\ 0 \\ 0 \end{pmatrix} \quad \mathbf{ub} = \begin{pmatrix} 1.5 \\ 2 \\ 1.5 \\ 2 \\ 3.5 \end{pmatrix}.$$

4) The objective function is expressed as

1160

$$\Psi = (-1 \quad -1 \quad 0 \quad 0 \quad 0) \begin{pmatrix} X_{12} \\ X_{13} \\ X_{24} \\ X_{34} \\ X_{45} \end{pmatrix}.$$

ACKNOWLEDGMENT

1161

The authors are grateful to Dr. S.-K. Chen and team, of the
 National Tsing Hua University in Taiwan, for their invaluable
 contribution.

1162
1163
1164

REFERENCES

1165

- [1] S. A. Eide, C. D. Gentillon, T. E. Wierman, and D. M. Rasmuson, "Reevaluation of station blackout risk at nuclear power plants," Tech. Rep. NUREG/CR-6890, U.S. Nuclear Regulatory Commission, Rockville, MD, USA, vol. 2, 2005. [Online]. Available: <https://www.nrc.gov/docs/ML0602/ML060200479.pdf> 1166
1167
1168
1169
- [2] S. A. Eide, C. D. Gentillon, T. E. Wierman, and D. M. Rasmuson, "Reevaluation of station blackout risk at nuclear power plants," Tech. Rep. NUREG/CR-6890, U.S. Nuclear Regulatory Commission, Rockville, MD, USA, vol. 1, 2005. [Online]. Available: <https://www.nrc.gov/docs/ML0602/ML060200477.pdf> 1170
1171
1172
1173
1174
1175
- [3] M. Čepin, "Event Tree Analysis," in *Assessment of Power System Reliability: Methods and Applications*. London, U.K.: Springer London, 2011, pp. 89–99. 1176
1177
1178
- [4] W. E. Vesely, F. F. Goldberg, N. H. Roberts, and D. F. Haasl, "Fault tree handbook," Tech. Rep. NUREG/CR-0492, U.S. Nuclear Regulatory Commission, Rockville, MD, USA, 1981. [Online]. Available: <https://www.nrc.gov/docs/ML1007/ML100780465.pdf> 1179
1180
1181
1182
- [5] M. Čepin, "Fault tree analysis," in *Assessment of Power System Reliability: Methods and Applications*. London, U.K.: Springer, 2011, pp. 61–87. 1183
1184
- [6] E. Ruijters and M. Stoelinga, "Fault tree analysis: A survey of the state-of-the-art in modeling, analysis and tools," *Comput. Sci. Rev.*, vol. 15, pp. 29–62, 2015. 1185
1186
1187
- [7] W. E. Vesely, M. Stamatelatos, J. Dugan, J. Fragola, J. Minarick, and J. Railsback, "Fault tree handbook with aerospace applications," Version 1.1, NASA Office of Safety and Mission Assurance, Washington, DC, USA, 2002. <https://www.hq.nasa.gov/office/codeq/doctree/fthb.pdf> 1188
1189
1190
1191
1192
- [8] F. I. Khan and S. Abbasi, "Analytical simulation and {PROFAT} ii: A new methodology and a computer automated tool for fault tree analysis in chemical process industries," *J. Hazardous Mater.*, vol. 75, no. 1, pp. 1–27, 2000. 1193
1194
1195
1196
- [9] S. K. Shin and P. H. Seong, "Review of various dynamic modeling methods and development of an intuitive modeling method for dynamic systems," *Nucl. Eng. Technol.*, vol. 40, no. 5, pp. 375–386, 2008. 1197
1198
1199
- [10] B. Kaiser, C. Gramlich, and M. Förster, "State/event fault trees: A safety analysis model for software-controlled systems," *Rel. Eng. Syst. Safety*, vol. 92, no. 11, pp. 1521–1537, 2007. 1200
1201
1202
- [11] Z. Zhou and Q. Zhang, "Model event/fault trees with dynamic uncertain causality graph for better probabilistic safety assessment," *IEEE Trans. Rel.*, vol. 66, no. 1, pp. 178–188, Mar. 2017. 1203
1204
1205
- [12] A. Bobbio, L. Portinale, M. Minichino, and E. Ciancamerla, "Improving the analysis of dependable systems by mapping fault trees into Bayesian networks," *Rel. Eng. Syst. Safety*, vol. 71, no. 3, pp. 249–260, 2001. 1206
1207
1208
1209

- 1210 [13] M. Čepin and B. Mavko, "A dynamic fault tree," *Rel. Eng. Syst. Safety*,
1211 vol. 75, no. 1, pp. 83–91, 2002.
- 1212 [14] J. B. Dugan, S. J. Bavuso, and M. A. Boyd, "Dynamic fault-tree models
1213 for fault-tolerant computer systems," *IEEE Trans. Rel.*, vol. 41, no. 3,
1214 pp. 363–377, Sep. 1992.
- 1215 [15] J. B. Dugan, S. J. Bavuso, and M. A. Boyd, "Fault trees and markov
1216 models for reliability analysis of fault-tolerant digital systems," *Rel. Eng.
1217 Syst. Safety*, vol. 39, no. 3, pp. 291–307, 1993.
- 1218 [16] K. D. Rao, V. Gopika, V. S. Rao, H. Kushwaha, A. Verma, and A. Srividya,
1219 "Dynamic fault tree analysis using Monte Carlo simulation in probabilistic
1220 safety assessment," *Rel. Eng. Syst. Safety*, vol. 94, no. 4, pp. 872–883,
1221 2009.
- 1222 [17] L. Meshkat, J. B. Dugan, and J. D. Andrews, "Dependability analysis of
1223 systems with on-demand and active failure modes, using dynamic fault
1224 trees," *IEEE Trans. Rel.*, vol. 51, no. 2, pp. 240–251, Jun. 2002.
- 1225 [18] J. B. Dugan, K. J. Sullivan, and D. Coppit, "Developing a low-cost high-
1226 quality software tool for dynamic fault-tree analysis," *IEEE Trans. Rel.*,
1227 vol. 49, no. 1, pp. 49–59, Mar. 2000.
- 1228 [19] C. Y. Huang and Y. R. Chang, "An improved decomposition scheme for
1229 assessing the reliability of embedded systems by using dynamic fault
1230 trees," *Rel. Eng. Syst. Safety*, vol. 92, no. 10, pp. 1403–1412, 2007.
- 1231 [20] L. F. Rocha, C. L. T. Borges, and G. N. Taranto, "Reliability evaluation of
1232 active distribution networks including islanding dynamics," *IEEE Trans.
1233 Power Syst.*, vol. 32, no. 2, pp. 1545–1552, Mar. 2017.
- 1234 [21] H. Lei and C. Singh, "Non-sequential Monte Carlo simulation for cyber-
1235 induced dependent failures in composite power system reliability evalua-
1236 tion," *IEEE Trans. Power Syst.*, vol. 32, no. 2, pp. 1064–1072, Mar.
1237 2017.
- 1238 [22] H. George-Williams and E. Patelli, "A hybrid load flow and event driven
1239 simulation approach to multi-state system reliability evaluation," *Rel. Eng.
1240 Syst. Safety*, vol. 152, pp. 351–367, 2016.
- 1241 [23] H. George-Williams and E. Patelli, "Maintenance strategy optimization for
1242 complex power systems susceptible to maintenance delays and operational
1243 dynamics," *IEEE Trans. Rel.*, vol. 66, no. 4, pp. 1309–1330, Dec. 2017.
- 1244 [24] H. George-Williams, M. Lee, and E. Patelli, "A framework
1245 for power recovery probability quantification in nuclear power
1246 plant station blackout sequences," in *Proc. Probabilistic Safety
1247 Assessment Manage. Conf.*, 2016, vol. 13. [Online]. Available:
1248 <http://iapsam.org/PSAM13/program/index4.php.htm>
- 1249 [25] A. Mosleh, D. M. Rasmuson, and F. M. Marshall, "Guidelines on model-
1250 ing common-cause failures in probabilistic risk assessment," Tech. Rep.
1251 NUREG/CR-5485, U.S. Nuclear Regulatory Commission, Rockville,
1252 MD, USA, 1998.
- 1253 [26] H. George-Williams and E. Patelli, "Efficient availability assessment of
1254 reconfigurable multi-state systems with interdependencies," *Rel. Eng. Syst.
1255 Safety*, vol. 15, pp. 431–444, 2017.
- 1256 [27] E. Patelli, "COSSAN: A multidisciplinary software suite for uncertainty
1257 quantification and risk management," in *Handbook of Uncertainty Quan-
1258 tification*. New York, NY, USA: Springer, 2017, pp. 1–69.
- 1259 [28] E. Patelli, M. Broggi, M. D. Angelis, and M. Beer, "Opencossan: An
1260 efficient open tool for dealing with epistemic and aleatory uncertainties,"
1261 in *Proc. 2nd Int. Conf. Vulnerability Risk Anal. Manag. 6th Int. Symp.
1262 Uncertainty Modeling Anal.*, 2014, pp. 2564–2573. [Online]. Available:
1263 <http://dx.doi.org/10.1061/9780784413609.258>
- Hindolo George-Williams** received the B.Eng.(Hons.) degree in electri- 1264
cal/electronic engineering from the University of Sierra Leone, Freetown, Sierra 1265
Leone, in 2010, and the M.Sc.(Eng.) degree in energy generation from the Uni- 1266
versity of Liverpool, Liverpool, U.K., in 2013. He is currently working toward 1267
the dual Ph.D. degree with the University of Liverpool and the National Tsing 1268
Hua University, Hsinchu, Taiwan. His Ph.D. research focuses on the probabilis- 1269
tic risk assessment of nuclear power plants. He was a Maintenance Engineer 1270
(for a period of 30 months) for the Sierra Leone affiliate of the French oil giant, 1271
TOTAL. 1272
- Mr. George-Williams received the Best Project Award from the Sierra Leone 1273
Institute of Engineers in recognition of his outstanding execution of his final 1274
B.Eng. project. 1275
1276
- Min Lee** received the Bachelor's and Master's degrees from the Department 1277
of Nuclear Engineering, NTHU, in 1977 and 1979, respectively, and the Ph.D. 1278
degree in nuclear engineering from the Massachusetts Institute of Technology, 1279
Cambridge, MA, USA, in 1985. 1280
- He is a Distinguished Professor with the Department of Engineering and 1281
System Science, National Tsing Hua University (NTHU), Hsinchu, Taiwan. 1282
He briefly worked at the Brookhaven National Laboratory after his Ph.D. and 1283
joined the Department of Engineering and System Science, NTHU, in 1989. He 1284
has held several administrative positions at NTHU, including Chairman of ESS 1285
Department, Vice President and Chief of Staff, Vice President of General Affairs, 1286
and Vice President of Student Affairs. He has also been on the board of directors 1287
of the Taiwan Power Company (a government-owned public utility) for 14 years 1288
and a member of the Nuclear Safety Committee of the same company for 12 1289
years. His research fields are probabilistic risk assessment of nuclear power 1290
plants, light water reactor severe accident phenomenology and management, 1291
source term characterization of nuclear power plants, heat transfer, and system 1292
thermal-hydraulic analyses of light water reactors. 1293
1294
- Edoardo Patelli** received the Graduate degree in nuclear engineering from the 1295
Politecnico di Milano, Milano, Italy. 1296
- He carried out his doctoral work in radiation science and technology from 1297
Politecnico di Milano in the group of Professor Marzio Marseguerra and Enrico 1298
Zio. He then moved as a Research Associate to the University of Innsbruck, 1299
Austria, in the group of Professor Schuëller. He is a Co-Principal Investigator 1300
of the Centre for Doctoral Training in Quantification and Management of Risk 1301
and Uncertainty in Complex Systems and Environments and a member of the 1302
Centre for Doctoral Training in "Next-Generation-Nuclear." He is a member of 1303
the Institute for Risk and Uncertainty, University of Liverpool, U.K., and an 1304
honorary member of the National Tsing Hua University, Hsinchu, Taiwan. He 1305
has published more than 200 contributions in international journals and pro- 1306
ceedings of international conferences. He has supervised more than 20 Ph.D. 1307
students on site and in collaboration with international partners. 1308
- Dr. Patelli is the Chair of the technical committee on simulation for safety 1309
and reliability analysis (European Safety and Reliability Association), a Guest- 1310
Editor of international journals (e.g., the International Journal of Reliability and 1311
Safety and Structural Safety), and has editorship of Springer's *Encyclopaedia of* 1312
Earthquake Engineering. He has also organized multidisciplinary international 1313
conferences on risk and vulnerability (e.g., ASCE-ICVRAM-ISUMA 2014, 1314
IPW2015) and a number of mini-symposia in different international confer- 1315
ences. 1316
1317